Article

Homeostatic mini-intestines through scaffold-guided organoid morphogenesis

https://doi.org/10.1038/s41586-020-2724-8

Received: 25 June 2018

Accepted: 24 June 2020

Published online: 16 September 2020

Check for updates

Mikhail Nikolaev[1], Olga Mitrofanova[1,7], Nicolas Broguiere[1,7], Sara Geraldo[1], Devanjali Dutta[1], Yoji Tabata[1], Bilge Elci[1], Nathalie Brandenberg[1,5], Irina Kolotuev[2], Nikolce Gjorevski[1,6], Hans Clevers[3] & Matthias P. Lutolf[1,4]✉

Epithelial organoids, such as those derived from stem cells of the intestine, have great potential for modelling tissue and disease biology[1–4]. However, the approaches that are used at present to derive these organoids in three-dimensional matrices[5,6] result in stochastically developing tissues with a closed, cystic architecture that restricts lifespan and size, limits experimental manipulation and prohibits homeostasis. Here, by using tissue engineering and the intrinsic self-organization properties of cells, we induce intestinal stem cells to form tube-shaped epithelia with an accessible lumen and a similar spatial arrangement of crypt- and villus-like domains to that in vivo. When connected to an external pumping system, the mini-gut tubes are perfusable; this allows the continuous removal of dead cells to prolong tissue lifespan by several weeks, and also enables the tubes to be colonized with microorganisms for modelling host–microorganism interactions. The mini-intestines include rare, specialized cell types that are seldom found in conventional organoids. They retain key physiological hallmarks of the intestine and have a notable capacity to regenerate. Our concept for extrinsically guiding the self-organization of stem cells into functional organoids-on-a-chip is broadly applicable and will enable the attainment of more physiologically relevant organoid shapes, sizes and functions.

We postulated that the morphogenetic processes that shape cystic intestinal organoids into their characteristic crypt and villus structures could be harnessed to promote in vitro stem cell patterning along predefined spatial boundaries, particularly those that approximate the three-dimensional (3D) topology of the surface of the gut. To this end, and inspired by previous work on micro-engineered intestinal surfaces[7,8], we generated a scaffold that would be permeable to gases, nutrients and macromolecules, that would facilitate the efficient adhesion, proliferation and differentiation of intestinal stem cells (ISCs) and that would be stiff enough to serve as a physical barrier restricting the growth of ISCs to predefined shapes. Whereas pure Matrigel was too soft to confine the growth of mouse ISCs (*LGR5-eGFP-IRES-creERT2* mouse model; hereafter, LGR5–eGFP$^+$ ISCs), we found that a hybrid matrix composed of a mixture of type-I collagen, which provides a relatively stiff, adhesive substrate, and Matrigel, which contains the key constituents of the native basement membrane, met the necessary requirements.

We integrated these hydrogels in a perfusable platform to generate a hybrid microchip system that consists of an elastomeric device with a central chamber for hydrogel loading and subsequent organoid culture, flanked by a pair of (inlet and outlet) reservoirs for cell loading and luminal perfusion, as well as lateral reservoirs that supply medium and growth factors to the basal side of the tissues through the hydrogel (Fig. 1a, b, Extended Data Fig. 1a). The microchannel, which contains microcavities that mimic the geometry of the native crypts in the mouse small intestine, was laser-ablated within the central gel scaffold (Fig. 1b, Extended Data Fig. 1b, c). These tubular hydrogel scaffolds could be readily colonized with mouse LGR5–eGFP$^+$ ISCs by perfusion from the inlet reservoir. Time-lapse microscopy showed the rapid establishment of a confluent cell sheet that was several times larger than organoids grown in 3D Matrigel (Fig. 1c, Supplementary Video 1). Confocal microscopy revealed a tightly packed, simple epithelium expressing high levels of E-cadherin at the junctions between cells (Extended Data Fig. 1d, Supplementary Video 2). These tissues remained open and free of cells at both ends, enabling the delivery of fluid to the apical side of the epithelium (Fig. 1d) and the removal of non-adherent or dead cells from the lumen (Fig. 1e). Notably, colonization of the tubular scaffolds by primary mouse cholangiocytes (Extended Data Fig. 2a), or by primary human stem and progenitor cells from the small intestine (Extended Data Fig. 2c–e) or trachea (Extended Data Fig. 2f, g), generated coherent, tightly packed and perfusable epithelial tissues. Trachea tubes could be readily cultured at the air–liquid interface (Extended Data Fig. 2f). Collectively, these data show that a scaffold that mimics the basement membrane can be used to reliably build—from primary stem and progenitor cells—openly accessible epithelia with an anatomy similar to that in vivo.

[1]Laboratory of Stem Cell Bioengineering, Institute of Bioengineering, School of Life Sciences (SV), École Polytechnique Fédérale de Lausanne (EPFL), Lausanne, Switzerland. [2]Electron Microscopy Facility, Faculty of Biology and Medicine, University of Lausanne, Lausanne, Switzerland. [3]Oncode Institute, Hubrecht Institute, Royal Netherlands Academy of Arts and Sciences and University Medical Center, Utrecht, The Netherlands. [4]Institute of Chemical Sciences and Engineering, School of Basic Sciences (SB), EPFL, Lausanne, Switzerland. [5]Present address: Startlab/SUN bioscience, Epalignes, Switzerland. [6]Present address: Roche Pharma Research and Early Development, Basel, Switzerland. [7]These authors contributed equally: Olga Mitrofanova, Nicolas Broguiere. ✉e-mail: matthias.lutolf@epfl.ch

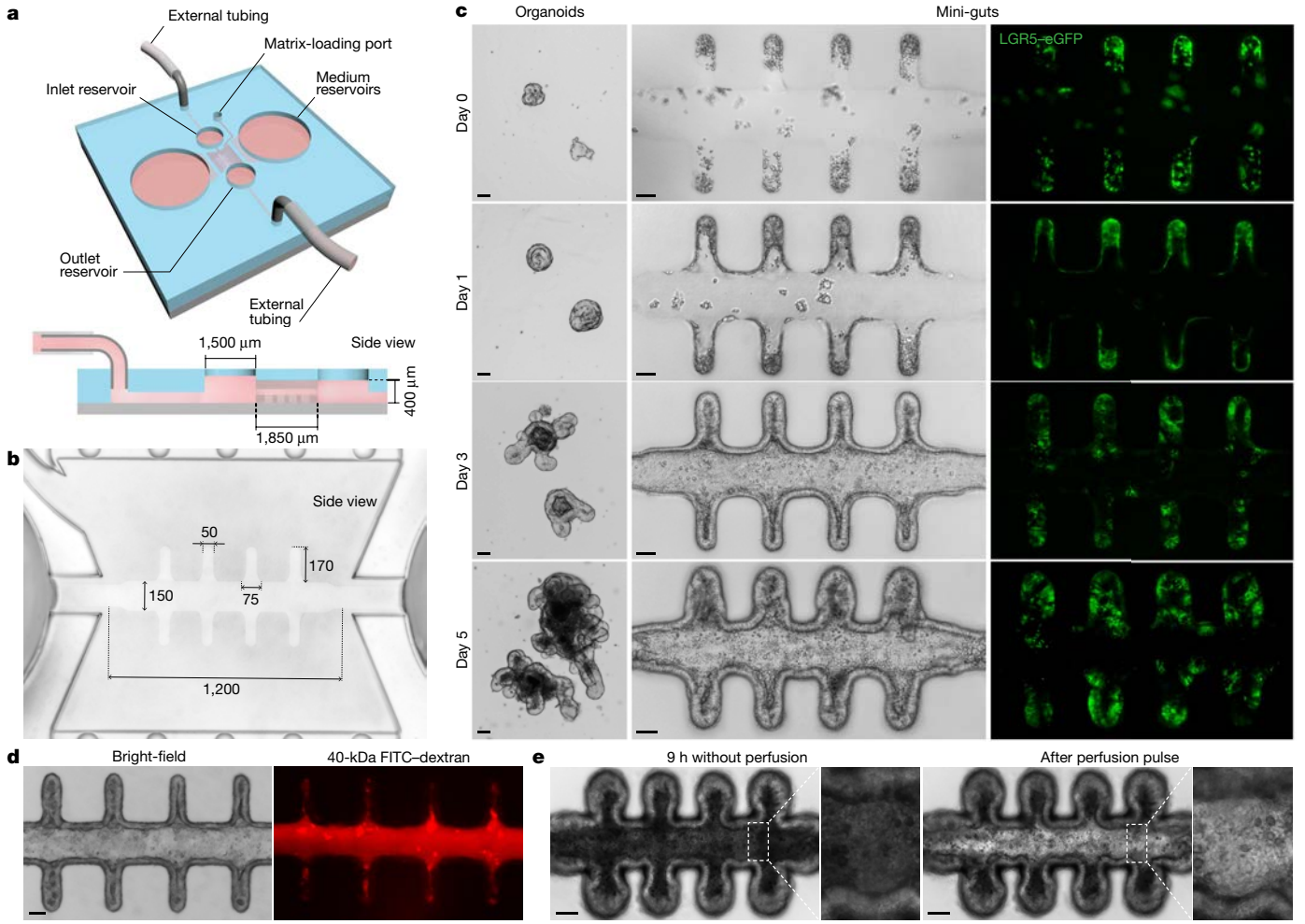

Fig. 1 | Establishment of long-term homeostatic culture of tubular mini-guts. a, Schematic of 3D hydrogel-containing microdevice developed for the mini-gut culture. The system consists of a hydrogel chamber in the centre flanked by two external medium reservoirs and two inlet and outlet reservoirs for perfusion through the lumen. **b**, Dimensions (in µm) of an open microchannel with an in vivo-like anatomical structure, generated by laser ablation. The channel spans the entire length of the central hydrogel compartment. **c**, Bright-field (left and middle) and LGR5–eGFP fluorescence (right) time-course experiments of epithelium formation in tissue-engineered mini-guts (middle and right) compared to traditional organoids formed in Matrigel (left). Extended depth of field of bright-field images, calculated for a *z*-stack of 80 µm; fluorescence confocal images correspond to a maximum intensity projection of a *z*-stack of around 60 µm. **d**, Bright-field and fluorescence confocal images of a five-day-old mini-gut tube perfused with fluorescein isothiocyanate (FITC)-tagged dextran (40 kDa), showing the maintenance of epithelium integrity. **e**, A 10-day-old mini-gut tube with accumulated dead cells that were shed into the lumen over the course of 9 h without perfusion (left), and just after a perfusion pulse (right). Scale bars, 50 µm.

Establishment of tissue homeostasis

Conventional epithelial organoids can be propagated nearly indefinitely, but long-term culture in these systems involves continuous passaging that requires breaking the organoids into fragments or dispersed single cells every few days[5]. We explored the possibility of maintaining tubular intestinal epithelia for several weeks without passaging; that is, by continuously removing dead cells from the rapidly growing epithelia through perfusion. Indeed, high levels of cell shedding and accumulation of dead cells in the closed cavity of conventional organoids led to tissue destruction after about 10 days (Extended Data Fig. 3a). In the absence of perfusion, the epithelial tubes became densely packed with dead cells after 6–10 hours (Fig. 1e, Supplementary Video 3), leading to tissue destruction a few days later (Extended Data Fig. 3c). Notably, when the lumen is perfused with standard organoid culture medium[5]—or even growth-factor-free medium—every 12 hours, to remove dead cells from the organoid tubes, the lifespan of the tissue could be extended to one month or longer, preserving the overall tissue anatomy and localized niches of LGR5–eGFP$^+$ ISCs (Extended Data Fig. 3d, e, Supplementary Video 4). Thus, our approach establishes—without the need for passaging—a long-living homeostatic organoid culture system in which cell birth and death are balanced.

Stereotypical cell-fate patterning

We next tested how the induction of differentiation would affect cell fate in ISC-derived epithelial tubes. Fluorescence imaging and immunostaining revealed a biomimetic spatial distribution of cell types (Fig. 2a–f, Supplementary Video 5), similar to the cell-fate patterns along the crypt–villus axis in vivo. We identified crypt-like regions that exclusively contained cells that stained positive for SOX9 (Fig. 2a) and the Paneth cell marker lysozyme (Fig. 2b). Labelling the dividing cells in the tissue with 5-ethynyl-2′-deoxyuridine (EdU) revealed distinct areas of cell proliferation that were to a large extent restricted to the crypt regions (Fig. 2c), whereas offspring cells migrated and replenished the short-lived differentiated cells in the intestinal lumen (Extended Data Fig. 4a)—mirroring the pattern seen in the native small intestine. By contrast, cells that stained positive for markers of enterocytes (Fig. 2d),

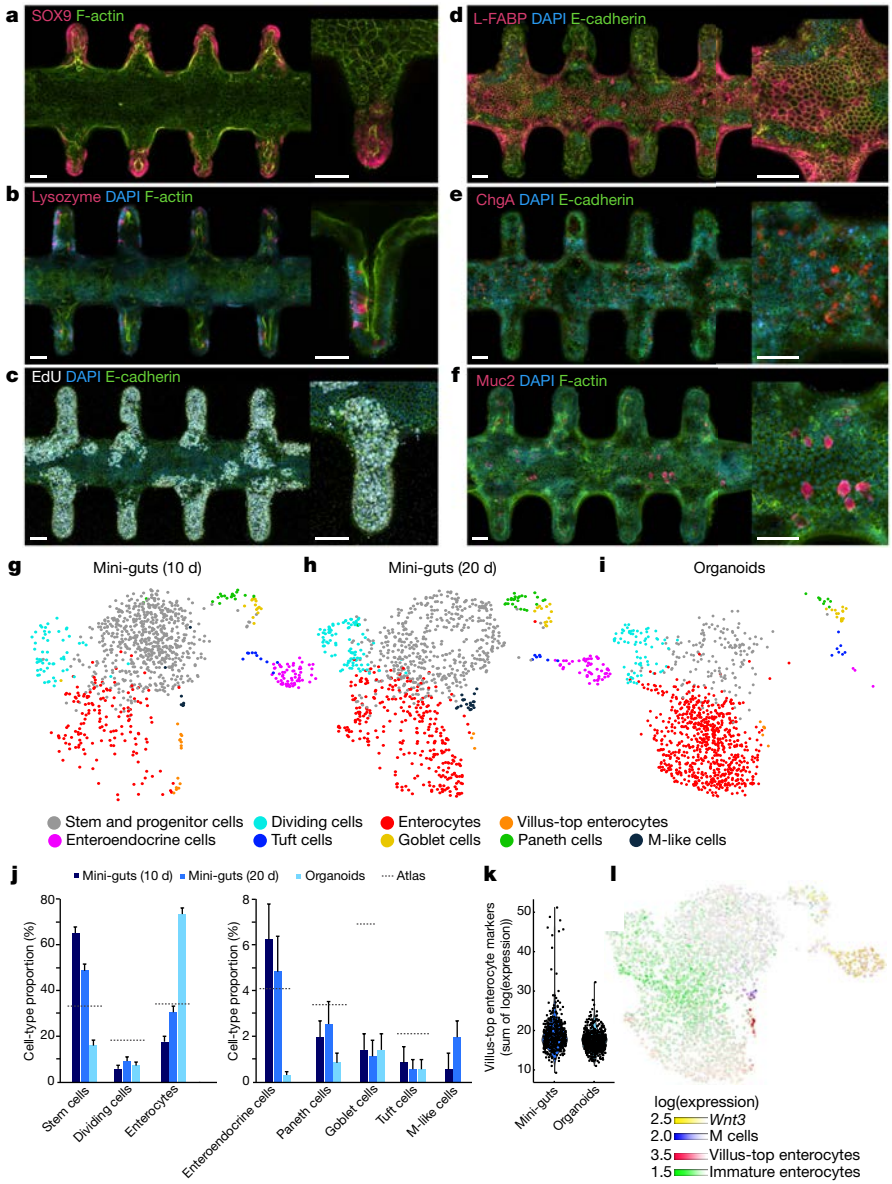

Fig. 2 | Cell-fate patterning and cellular diversity of tubular mini-guts. a–f, Fluorescence confocal images of representative 7-day-old mini-gut tubes, showing an entire tissue (left) and a higher-magnification view (right), containing: SOX9$^+$ stem and progenitor cells (red, **a**); lysozyme$^+$ Paneth cells (red, **b**); proliferating cells following an EdU pulse of 12 h (white, **c**); L-FABP$^+$ enterocytes (red, **d**); chromogranin A (ChgA)$^+$ enteroendocrine cells (red, **e**); and mucin 2 (Muc2)$^+$ goblet cells (red, **f**). Nuclei are stained with DAPI (blue) and cellular actin filaments are stained with E-cadherin or phalloidin (green). Images correspond to the maximum intensity projection of a *z*-stack of around 60 µm. Scale bars, 50 µm. Data in **a**–**f** are representative of at least two independent experiments. **g**–**i**, Unsupervised clustering of the key intestinal epithelial cell types in 10-day-old mini-guts (**g**), 20-day-old mini-guts (**h**) and classical 3D organoids (**i**). **j**, Cell-type proportions in conventional organoids and mini-guts, compared to in vivo data ('atlas')[9]. Error bars are 95% confidence intervals estimated from theoretical sampling error. **k**, Expression of villus-top enterocyte marker genes in mini-guts and organoids (sum of a published signature of 42 genes)[13]. Each point represents a cell. **l**, Overlay of averaged values of marker genes that define M cells (*Zmat3*, *Mmp15*, *Myadm*, *Anxa5* and *Marcksl1*), immature enterocytes (*Fgfbp1*, *Dmbt1*, *Pdss1* and *Prss32*) and villus-top enterocytes (*Ada*, *Ifrd1*, *Krt20*, *Pmp22* and *Serpinb1a*). log(expression) refers to the natural logarithm of count values normalized to 10,000 per cell.

enteroendocrine cells (Fig. 2e) and goblet cells (Fig. 2f) were found almost exclusively in the central regions of the tubes, which correspond to villus-like areas.

For the organoids to be representative of the native intestinal mucosa, they must sustain its secretory and absorptive function. To test this, we removed epithelia from the microchips for downstream histological sectioning and analyses (Extended Data Fig. 4b). Alcian blue staining of acidic mucopolysaccharides identified goblet cells and a thin mucus layer covering the apical side of the epithelium (Extended Data Fig. 4c). Transmission electron microscopy (TEM) analysis confirmed the presence of cells with mucus-containing secretory vesicles, together with a single layer of densely packed enterocytes with their characteristic microvilli forming a brush border on the apical surface (Extended Data Fig. 4d). An analysis of the function of brush border aminopeptidases—the enzymes that are responsible for the final step in the digestion of dietary carbohydrates and proteins—showed that enzymatic activity increased steadily after the induction of differentiation, until a plateau was reached four days later that was sustained in longer-lived tissues (Extended Data Fig. 4e). Together, these data show that a spatially confining hydrogel scaffold promotes the 'guided' self-organization of ISCs into a functional intestinal epithelium that exhibits a spatial arrangement of crypt- and villus-like domains similar to that in vivo.

Emergence of rare cell types

To shed light on the cellular diversity and the proportions of different cell types that are found in mini-gut tubes, we performed a single-cell RNA sequencing (scRNA-seq) analysis of cells isolated from young (10 days) and older (20 days) mini-guts, as well as pooled Matrigel-derived organoids (Fig. 2g–l). On the basis of previously described cell-type markers in the endogenous intestinal epithelium[9], we defined nine main transcriptionally distinct clusters that correspond to the key cell types found in vivo (Fig. 2g–j, Extended Data Fig. 5). Consistent with the maintenance of a crypt-like domain (Fig. 2a, c, Extended Data Fig. 3a, b), we found that mini-guts retained a relatively large proportion of stem and progenitor cells (around 50% after 20 days) compared to conventional organoids (around 15%). Notably, from day 10 to day 20, a progressive shift in the fraction of stem and progenitor cells to enterocytes was apparent (Fig. 2g, h), suggesting that tissue maturation was occurring in the homeostatic mini-gut tubes. The proportions of dividing cells (around 5–10%), Paneth cells (around 1–2%) and Tuft cells (around 0.5–1%) were similar in organoids and mini-gut tubes, and approximated the proportions in endogenous tissues[9] (Fig. 2j, Extended Data Fig. 6a–i). Compared to the in vivo condition, the proportion

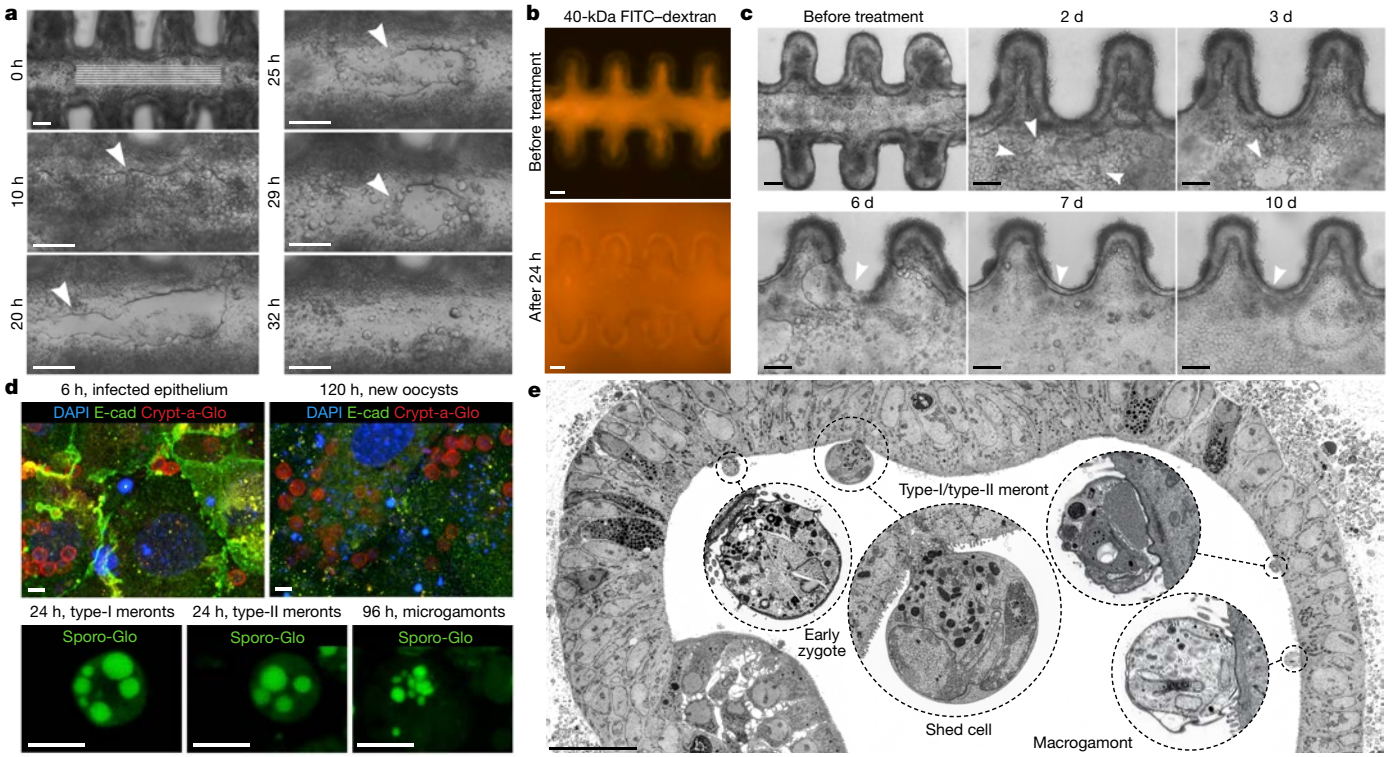

Fig. 3 | Perspectives for modelling intestine biology and disease. **a**, Epithelial wound healing in mini-gut tubes damaged by targeted laser ablation. **b**, DSS-induced loss of intestinal barrier integrity, as shown by FITC–dextran permeability. **c**, Time-course experiments of DSS-induced epithelial damage and regeneration. Arrowheads indicate regeneration of the lesion areas (**a**, **c**). Scale bars, 50 µm (**a**–**c**). Data in **a**–**c** are representative of at least three independent experiments. **d**, Immunofluorescence of *C. parvum* undergoing its major epicellular stages in the mini-guts. After about 6 h of infection, floating half-empty oocysts were observed; at 24–72 h after infection type-I and type-II meronts were detected; at 72–96 h microgamonts containing 12–16 microgametes were detected; and at 120–144 hours new oocysts were again observed, implying that the parasite was able to complete its full life cycle within the mini-gut lumen. Nuclei of intestinal epithelial cells are stained with DAPI (blue) and cellular actin filaments E-cadherin (green). The different stages of the *C. parvum* life cycle are stained with Crypt-a-Glo (oocyst outer walls; red) and Sporo-Glo (sporozoites, merozoites and all other intracellular reproductive stages; green). Scale bars, 5 µm. **e**, Scanning electron microscopy image of distinct stages of the *C. parvum* life cycle at 72 h after infection. Scale bar, 25 µm. Data in **d**, **e** are representative of two independent experiments and at least 10 different mini-gut tube regions were analysed.

of Goblet cells was much lower in both in vitro conditions (around 7% in vivo; 1% in vitro) (Fig. 2j).

A few rare and functionally important specialized cell types are difficult to reproduce in intestinal organoid cultures[9–11], as they generally require specific manipulations that may disrupt stereotypical organoid patterning along a crypt–villus axis. These cell types include microfold cells (M cells), which are crucial players in mucosal immunity[12]; a subset of enterocytes found specifically near the tip of intestinal villi that also have immune-modulatory functions[13]; and enteroendocrine cells, which are the main sources of gut-derived hormones. Cells that express villus-top enterocyte markers[13] were found in mini-guts but not in traditional organoids (Fig. 2g–l). They shared some traits with a cluster of rare cells (0.5–2%) positive for marker genes that define immature M cells (*Marcksl1* and *Anxa5*), so-called revival stem cells[14] (*Clu* and *Msln*) and regenerating cells[15] (*Ly6a*) of the intestinal epithelium (Fig. 2g–l, Extended Data Fig. 7). These M-like cells were not detected in control organoids and expressed a unique set of genes characteristic of M-cell function in vivo (Extended Data Fig. 7a). Their presence in the mini-guts was confirmed by immunostaining for the universal M-cell marker GP2[14] (Extended Data Fig. 7b). Notably, enteroendocrine cells are relatively abundant (around 5%) in homeostatic mini-guts, resembling the cell fraction found in vivo (Fig. 2j) and capturing the hormone expression profile of key enteroendocrine cell types (Extended Data Fig. 7c). By contrast, these cells are exceedingly rare in conventional organoids (around 0.3%), unless organoid differentiation is promoted through treatment with inhibitors of the Wnt, Notch or EGF pathways[11]. Collectively, these data show that the diversity of cell types in our homeostatic mini-guts closely resembles that of the intestinal epithelium in vivo, and includes cell types that are rare or absent in conventional organoids.

Regenerative potential of mini-gut tubes

We next tested the extent to which tubular mini-guts could regenerate after an injury induced by three models of epithelial damage. First, we used an ultraviolet laser beam to introduce epithelial lesions at defined locations (Fig. 3a, Supplementary Video 6). Because of the stability of the mini-gut tubes, we could readily track tissue repair by live-cell microscopy; this revealed an invasion of cells from the surrounding tissue that resulted in complete regeneration in less than 32 hours. Next, we treated the tissues with dextran sodium sulfate (DSS), a cytotoxic compound that is frequently used to model ulcerative colitis in mice[16]. In contrast to conventional organoids, which rapidly collapsed in response to treatment with DSS (Supplementary Video 7), the mini-gut tubes showed a notable ability to regenerate (Fig. 3b, c)—probably owing to the more physiological luminal exposure of the tissues to the toxic polysaccharide. Finally, to mimic the intestinal damage and regeneration that occurs in vivo, we exposed the mini-guts to γ-radiation (Extended Data Fig. 8a, Supplementary Video 8). Exposure to a high dose of radiation (8 Gy) resulted in a loss of stem cells and impaired regeneration (Extended Data Fig. 8a, b). At a lower dose (2 Gy), we observed a rapid depletion of proliferating ISCs and a disruption of the intestinal epithelium, followed by a gradual re-epithelialization until the tissue was completely regenerated with newly established crypts (Extended Data Fig. 8b, c). Together, these

experiments reveal that our bioengineered organoids show notable regenerative potential.

Modelling long-term parasite infection

Finally, we investigated whether mini-gut tubes could be used to model long-term infection caused by *Cryptosporidium parvum*, an obligate parasite that results in life-threatening diarrhoea in immunocompromised adult hosts and in infants[17]. Research on the pathophysiology of *C. parvum* has been hindered by the lack of long-term, primary-cell-derived in vitro culture systems. Conventional 3D organoids can be used to model *C. parvum* infection[18], but the luminal inaccessibility and inability of the system to support long-term host–microorganism co-cultures limit the applicability of this system.

We infected mini-gut tubes with *C. parvum* by loading a suspension of oocysts into the inlet reservoir of the microchip (Extended Data Fig. 9a). Live-cell microscopy demonstrated that the tubular organoids support the completion of the life cycle and long-term growth of *C. parvum* without compromising tissue integrity (Extended Data Fig. 9b, Supplementary Video 9). The identity of each asexual and sexual stage was confirmed using immunofluorescence assays (Fig. 3d) and TEM imaging on mini-gut cross-sections (Fig. 3f, Extended Data Fig. 9c, d). By infecting mini-guts with freshly isolated sporozoites and analysing the luminal content every day, we observed successive rounds of production of newly formed oocysts for at least four weeks (Extended Data Fig. 9e). Gene set enrichment analysis of infected samples showed a significant enrichment of interferon-α response genes, as well as changes in metabolism (Extended Data Fig. 9f). An analysis by cell type showed that the interferon response was not limited to one specific population, but was instead distributed across all cell types, even though the response genes showed some cell-type specificities (Extended Data Fig. 9g; see also Source Data). Altogether, these results show that these bioengineered organoids, similar to primary-stem-cell-derived intestinal monolayers comprising feeder cells[19], are ideally suited for mechanistic host–microorganism interaction and long-term infection studies.

By combining bioengineering with the self-organization properties of stem cells, here we have generated open, tubular 'organoids-on-a-chip' that exhibit exceptional cell-type diversity, tissue architecture and function. The introduction of a microchip-based perfusion system made it possible to efficiently remove shed cells from the lumen and expose it to parasites or medium additives. Previous efforts to model intestinal epithelia through micro-engineering or tissue engineering[7,8,19–25] have successfully addressed the problem of lumen accessibility, but it has not yet been possible in these systems to capture the diversity of cell types and the patterning that are found in vivo or in classical organoids. Moreover, existing approaches are based on polarized cell monolayers grown on two-dimensional permeable polymer membranes[26,27], which may preclude the modelling of complex 3D multi-tissue interactions. The biomimetic 3D extracellular matrix that surrounds the patterned intestinal epithelium in our system can be readily colonized with non-epithelial cell types (Extended Data Fig. 10a) such as endothelial cells (Extended Data Fig. 10b), immune cells (Extended Data Fig. 10c, d) and myofibroblasts (Extended Data Fig. 10e, f). These supportive cell types were found to communicate with intestinal epithelial cells; for example, macrophages were observed to undergo morphological changes and ingest particles excreted from the epithelium (Extended Data Fig. 10c, Supplementary Video 10). The functional integration of an immune axis in bioengineered, homeostatic organoids opens up new perspectives for disease modelling. We anticipate that by adjusting specific characteristics of the hydrogel scaffolds (for example, their composition, geometry, size, stiffness and signalling inputs), the approach we describe here could be applied to other organoid-forming stem cells—including those derived from other organs, such as the lung, liver or pancreas, and derived from patient biopsies (Extended Data Fig. 2). The readily accessible 3D tissue anatomy of our model, which captures the development of stem cells in a highly tractable experimental framework, will answer questions that have so far been difficult to address, and may have substantial potential for drug discovery, diagnostics and regenerative medicine.

Online content

Any methods, additional references, Nature Research reporting summaries, source data, extended data, supplementary information, acknowledgements, peer review information; details of author contributions and competing interests; and statements of data and code availability are available at https://doi.org/10.1038/s41586-020-2724-8.

1. Clevers, H. Modeling development and disease with organoids. *Cell* **165**, 1586–1597 (2016).
2. Sato, T. & Clevers, H. Growing self-organizing mini-guts from a single intestinal stem cell: mechanism and applications. *Science* **340**, 1190–1194 (2013).
3. Dekkers, J. F. et al. A functional CFTR assay using primary cystic fibrosis intestinal organoids. *Nat. Med.* **19**, 939–945 (2013).
4. van de Wetering, M. et al. Prospective derivation of a living organoid biobank of colorectal cancer patients. *Cell* **161**, 933–945 (2015).
5. Sato, T. et al. Single Lgr5 stem cells build crypt-villus structures in vitro without a mesenchymal niche. *Nature* **459**, 262–265 (2009).
6. Gjorevski, N. et al. Designer matrices for intestinal stem cell and organoid culture. *Nature* **539**, 560–564 (2016).
7. Wang, Y. et al. Formation of human colonic crypt array by application of chemical gradients across a shaped epithelial monolayer. *Cell. Mol. Gastroenterol. Hepatol.* **5**, 113–130 (2018).
8. Wang, Y. et al. A microengineered collagen scaffold for generating a polarized crypt-villus architecture of human small intestinal epithelium. *Biomaterials* **128**, 44–55 (2017).
9. Haber, A. L. et al. A single-cell survey of the small intestinal epithelium. *Nature* **551**, 333–339 (2017).
10. de Lau, W. et al. Peyer's patch M cells derived from Lgr5$^+$ stem cells require SpiB and are induced by RankL in cultured "miniguts". *Mol. Cell. Biol.* **32**, 3639–3647 (2012).
11. Basak, O. et al. Induced quiescence of Lgr5$^+$ stem cells in intestinal organoids enables differentiation of hormone-producing enteroendocrine cells. *Cell Stem Cell* **20**, 177–190 (2017).
12. Hase, K. et al. Uptake through glycoprotein 2 of FimH$^+$ bacteria by M cells initiates mucosal immune response. *Nature* **462**, 226–230 (2009).
13. Moor, A. E. et al. Spatial reconstruction of single enterocytes uncovers broad zonation along the intestinal villus axis. *Cell* **175**, 1156–1167 (2018).
14. Ayyaz, A. et al. Single-cell transcriptomes of the regenerating intestine reveal a revival stem cell. *Nature* **569**, 121–125 (2019).
15. Yui, S. et al. YAP/TAZ-dependent reprogramming of colonic epithelium links ECM remodeling to tissue regeneration. *Cell Stem Cell* **22**, 35–49 (2018).
16. Kiesler, P., Fuss, I. J. & Strober, W. Experimental models of inflammatory bowel diseases. *Cell. Mol. Gastroenterol. Hepatol.* **1**, 154–170 (2015).
17. Kotloff, K. L. The burden and etiology of diarrheal illness in developing countries. *Pediatr. Clin. North Am.* **64**, 799–814 (2017).
18. Heo, I. et al. Modelling *Cryptosporidium* infection in human small intestinal and lung organoids. *Nat. Microbiol.* **3**, 814–823 (2018).
19. Wilke, G. et al. A stem-cell-derived platform enables complete *Cryptosporidium* development in vitro and genetic tractability. *Cell Host Microbe* **26**, 123–134 (2019).
20. Kim, H. J., Huh, D., Hamilton, G. & Ingber, D. E. Human gut-on-a-chip inhabited by microbial flora that experiences intestinal peristalsis-like motions and flow. *Lab Chip* **12**, 2165–2174 (2012).
21. Kasendra, M. et al. Development of a primary human Small Intestine-on-a-Chip using biopsy-derived organoids. *Sci. Rep.* **8**, 2871 (2018).
22. Trietsch, S. J. et al. Membrane-free culture and real-time barrier integrity assessment of perfused intestinal epithelium tubes. *Nat. Commun.* **8**, 262 (2017).
23. Chen, Y., Zhou, W., Roh, T., Estes, M. K. & Kaplan, D. L. In vitro enteroid-derived three-dimensional tissue model of human small intestinal epithelium with innate immune responses. *PLoS ONE* **12**, e0187880 (2017).
24. Workman, M. J. et al. Enhanced utilization of induced pluripotent stem cell-derived human intestinal organoids using microengineered chips. *Cell. Mol. Gastroenterol. Hepatol.* **5**, 669–677 (2018).
25. Wang, Y. et al. Long-term culture captures injury-repair cycles of colonic stem cells. *Cell* **179**, 1144–1159 (2019).
26. Bhatia, S. N. & Ingber, D. E. Microfluidic organs-on-chips. *Nat. Biotechnol.* **32**, 760–772 (2014).
27. Wang, Y. et al. Bioengineered systems and designer matrices that recapitulate the intestinal stem cell niche. *Cell. Mol. Gastroenterol. Hepatol.* **5**, 440–453 (2018).

Methods

Data reporting

No statistical methods were used to predetermine sample size. The experiments were not randomized. The investigators were not blinded to allocation during experiments and outcome assessment unless otherwise stated.

Mice

Intestinal crypts, bile ducts and intestinal myofibroblasts were extracted from 5–10-week-old heterozygous LGR5-eGFP-IRES-CreERT2 or wild-type C57BL/6J mice (Jackson Laboratory), following animal experimentation protocols prescribed by EPFL and the Federation for Laboratory Animal Science Association (FELASA), in compliance with local animal welfare laws, guidelines and policies.

Isolation of intestinal crypts

Mouse intestinal crypts and single LGR5–eGFP ISCs were isolated following previously described procedures. In brief, the proximal part of the intestine was collected, opened longitudinally and washed with ice-cold phosphate-buffered saline (PBS). The luminal side of the intestine was scraped using a glass slide to remove luminal content and villous structures. After a second wash with ice-cold PBS, the intestine was cut into 2–4-mm pieces with scissors. The pieces were transferred to a tube and further washed with cold PBS (5–10 times) with gentle vortexing. Intestinal fragments were incubated in PBS containing 20 mM EDTA, for 20 min on ice. The supernatant was discarded and cold PBS was added to the fragments. Crypts were released by manual shaking of the suspension for 5 min. The supernatant was collected and passed through a 70-μm strainer. The remaining tissue fragments were again resuspended in cold PBS and triturated 5–10 times, and the supernatant was passed through a 70-μm strainer. The previous step was repeated once again. The three crypt-containing fractions were pooled together and centrifuged at 110*g* for 5 min. The pellet was resuspended in cold Advanced Dulbecco's modified Eagle medium/Ham's F-12 (Advanced DMEM/F12) supplemented with 1× Glutamax, 10 mM HEPES and 100 μg ml^{-1} penicillin–streptomycin (Gibco), and centrifuged at 84*g* to remove single cells and tissue debris. Crypts were then cultured according to the mouse intestinal organoids culture protocol (see 'Cell culture'), and after three passages single viable LGR5–eGFP^{high} cells were sorted by flow cytometry.

Cell culture

The following medium formulations were used in the protocol: base medium (BM) was prepared from Advanced DMEM/F12 medium supplemented with 1× Glutamax, 10 mM HEPES and 100 μg ml^{-1} penicillin–streptomycin (Gibco); BMGF medium was prepared from BM supplemented with 1× B27 supplement, 1× N2 supplement (Gibco) and 1 mM *N*-acetylcysteine (Sigma-Aldrich); ISC expansion medium (ENRCV) was prepared from BMGF supplemented with growth factors (50 ng ml^{-1} EGF (E) (Peprotech), 100 ng ml^{-1} Noggin (N) (EPFL Protein Expression Core Facility), 500 ng ml^{-1} R-Spondin 1 (R) (EPFL Protein Expression Core Facility)) and small molecules (3 μM CHIR99021 (C) (Stemgent) and 1 mM valproic acid (V) (Sigma-Aldrich)).

Isolated crypts or single cells were embedded in Matrigel (Corning; growth-factor-reduced, phenol-red-free formulation) and cast into 25-μl droplets in a 24-well plate. After polymerization of Matrigel (15 min, 37 °C), 500 μl of ENRCV medium was added. For freshly extracted mouse crypts and single-cell culture, 2.5 μM Thiazovivin (Stemgent) was included in ENRCV medium for the first two days to prevent anoikis. Fresh medium was replenished every other day. For passage, organoids were removed from Matrigel and mechanically dissociated into smaller fragments, and then transferred to fresh Matrigel. Passaging was performed every fourth day with a 1:4 split ratio. Organoids were used for experiments between passage number 5 and 20. A detailed protocol describing organoid culture has been deposited in the Protocol Exchange repository[28].

Intestinal myofibroblasts were isolated from C57BL/6J mice following a previously published protocol with slight modifications[29]. Mouse small intestinal tissue was processed and used for intestinal crypt isolation as described above. Remaining intestinal fragments were then washed and incubated in DMEM containing collagenase IV (300 U ml^{-1}; Invitrogen) and dispase (0.08 U ml^{-1}; Roche) for 30 min at 37 °C in a shaking water bath. The supernatant was then collected, centrifuged at 280*g* for 5 min and resuspended in DMEM supplemented with 10% heat-inactivated fetal bovine serum (HI-FBS), 100 μg ml^{-1} penicillin–streptomycin, 1× L-glutamine, 1× non-essential amino acids, 1× insulin–transferrin–selenium (Gibco) and 1× Primocin (InvivoGen). Cells were then transferred to T75 culture flasks, and the medium was changed after cell attachment (4–5 h) and every two days. Cells were split 1:2 as needed and used between passage 3 and 8.

Collected liver tissues were minced and digested as previously described[30]. In brief, whole liver was incubated in collagenase XI (0.012%), dispase (0.012%) and FBS (1%) in Advanced DMEM/F12 with 100 μg ml^{-1} penicillin–streptomycin, 1× Glutamax and 10 mM HEPES (Gibco), termed BM, for 2–3 h until bile duct fragments were visible. Remaining tissue pieces were let to sediment by gravitation and supernatant containing ductal fragments was collected and centrifuged at 200 rpm for 4 min and washed with PBS. Isolated fragments were resuspended in Matrigel (Corning; growth-factor-reduced, phenol-red-free formulation) and cast into 25-μl droplets in a 24-well plate. Following polymerization of Matrigel, 500 μl of isolation medium, containing BM supplemented with 1× B27 supplement, 1× N2 supplement (Gibco), 1.25 μM *N*-acetylcysteine (Sigma-Aldrich), 10 nM gastrin (Sigma-Aldrich) and growth factors (50 ng ml^{-1} EGF (Peprotech), 1 μg ml^{-1} R-Spondin 1 (EPFL Protein Expression Core Facility), 100 ng ml^{-1} FGF-10 (Peprotech), 10 mM nicotinamide (Sigma-Aldrich), 50 ng ml^{-1} HGF (Peprotech), 1 μg ml^{-1} WNT3A (Time Bioscience), 100 ng ml^{-1} Noggin (EPFL Protein Expression Core Facility) and 10 μM Y-27632 (Sigma-Aldrich) was added. After four days of culture, the medium was changed to expansion medium (EM) composed of isolation medium without WNT3A, Noggin and Y-27632. Organoids were passaged by mechanical dissociation every 10–14 days in split ratio 1:4 to 1:8.

The use of human embryonic stem (ES) cell lines was authorized by the Office Fédéral de la Santé Publique (OFSP) after approval by the cantonal ethical commission (CER-VD). All the experiments reported in this Article were performed under authorization number R-FP-S-2-0014-0000. HES3 MIXL1$^{GFP/+}$ human ES cells were obtained from A. G. Elefanty (Murdoch Children's Research Institute) and routinely maintained in mTeSR1 medium (StemCell Technologies) on 6-well plates coated with Matrigel human ES cell-qualified matrix (Corning). The medium was changed every day. For routine culture the cells were passaged every 4–5 days as small clumps using the Gentle Cell Dissociation Reagent (StemCell Technologies).

Macrophages were generated from HES3 MIXL1$^{GFP/+}$ human ES cells as previously described[31].In brief, during the first two days of differentiation, human ES cell colonies were specified to the mesoderm by incubation in StemPro Medium (Gibco) with 5 ng ml^{-1} BMP4, 50 ng ml^{-1} VEGF (Peprotech) and 2 μM CHIR99021 (Stemgent). In the next step (day 2–4) human haemangioblast-like cell formation was induced by replacing CHIR99021 with 20 ng ml^{-1} hbFGF (Peprotech) and later (day 4–6) maintained with VEGF and hbFGF only. The cells were then cultured for the next 16 days in StemPro Medium for haematopoietic stem cell differentiation with the following cytokines: differentiation day 6: 10 ng ml^{-1} VEGF, 10 ng ml^{-1} hbFGF, 50 ng ml^{-1} SCF, 30 ng ml^{-1} DKK-1, 20 ng ml^{-1} IL-3, 20 ng ml^{-1} TPO and 20 ng ml^{-1} FLT3 (Peprotech); differentiation day 8 and 10: 10 ng ml^{-1} VEGF, 10 ng ml^{-1} hbFGF, 50 ng ml^{-1} SCF, 30 ng ml^{-1} DKK-1, 20 ng ml^{-1} IL-3, 20 ng ml^{-1} TPO and 20 ng

ml^{-1} FLT3); differentiation day 12 and 14 (10 ng ml^{-1} hbFGF, 50 ng ml^{-1} SCF, 20 ng ml^{-1} IL-3, 20 ng ml^{-1} TPO and 20 ng ml^{-1} FLT3). Replating was performed starting from day 8 until day 22. The medium with cells was collected and centrifuged at 900*g* for 4 min. The resulting cell pellet was resuspended in fresh medium (1 ml per well) and plated into 6-well plates. From differentiation day 16, for myeloid differentiation the cells were switched to serum-free differentiation (SF-Diff) medium supplemented with 50 ng ml^{-1} hbFGF, and a full medium change was done every three days up to differentiation day 25, when the floating cells were collected and used for experiments. SF-Diff medium consisted of 50% IMDM, 50% DMEM/F12 with Glutamax, 1× N2 supplement, 1× B27 supplement, 0.5% cell-culture grade bovine serum albumin (BSA) and 100 µg ml penicillin–streptomycin (Gibco). StemPro Medium consisted of StemPro-34 SFM (Gibco), supplemented with 0.5 mM ascorbic acid (Sigma-Aldrich) and 100 µg ml^{-1} penicillin–streptomycin (Gibco).

Human small intestinal organoids cryopreserved at passage 8 were provided by the H. Clevers laboratory (Hubrecht Institute) within the framework of collaboration agreements. Small intestinal organoids were established from duodenal biopsy samples from healthy human donors as previously described[32]. Endoscopic biopsies were performed at the University Medical Center Utrecht and the Wilhelmina Children's Hospital. The patients' informed consent was obtained, and this study was approved by the ethical committee of the University Medical Center Utrecht. Human small intestinal organoids were cultured in human ISC expansion medium composed of 50% L-WRN conditioned medium (1:1 dilution with BM) supplemented with 1× B27 supplement (Gibco), 1 µM *N*-acetylcysteine (Sigma-Aldrich), 50 ng ml^{-1} EGF (Peprotech), 500 nM A83-01 (Tocris), 10 nM gastrin (Sigma-Aldrich), 10 mM nicotinamide (Sigma-Aldrich), 10 µM SB202190 (Seleckchem), 10 nM prostaglandin E2 (Tocris). Y-27632 (10 µM; Seleckchem) was used in the first 48 h after single-cell dissociation to prevent detachment-induced cell apoptosis. L-WRN conditioned medium was prepared from L-WRN cells (CRL-3276; ATCC) following a published protocol[33]. The medium was changed every two days and the expanding organoids were passaged by mechanical dissociation using a fire-polished glass Pasteur pipette every six to eight days.

Airway organoids were generated using healthy residual tissue from patients undergoing segmentary tracheal resection at the Centre Hospitalier Universitaire Vaudois (CHUV). The patients' informed consent was obtained before sampling, and the use of anonymized tissue samples for in vitro organoid culture was approved by the cantonal ethical commission (CER-VD). Tracheal tissue was dissociated using previously published protocols[34,35]. In brief, tissue was minced and digested in airway organoid medium supplemented with 2 mg ml^{-1} collagenase (Sigma-Aldrich, C9407) on an orbital shaker at 37 °C for 3 h. Airway organoid medium was prepared from Advanced DMEM/F12 with 1× Glutamax, 10 mM HEPES, 100 µg ml^{-1} penicillin–streptomycin, 1× B27 supplement (Gibco), 1× Primocin (Invivogen) and 1.25 mM *N*-acetylcysteine (Sigma-Aldrich) supplemented with 100 ng ml^{-1} Noggin (EPFL Protein Expression Core Facility), 500 ng ml^{-1} R-Spondin 1 (EPFL Protein Expression Core Facility), 25 ng ml^{-1} FGF-7 (Peprotech), 100 ng ml^{-1} FGF-10 (Peprotech), 500 nM A83-01 (Tocris), 5 mM nicotinamide (Sigma-Aldrich), 10 µM SB202190 (Seleckchem) and 5 µM Y-27632 (Seleckchem). The digested tissue suspension was sheared using flamed glass Pasteur pipettes several times. After each shearing step, the suspension was sequentially strained over a 100-µm filter and 2% FBS was added to the strained suspension before centrifugation at 400*g*. Erythrocytes were lysed in 2 ml red blood cell lysis buffer (Roche) for 5 min at room temperature. After centrifugation at 400*g* the resulting cell pellets were resuspended in Matrigel and cultured in airway organoid medium. The medium was changed every four days and organoids were passaged by mechanical dissociation using a fire-polished glass Pasteur pipette every two weeks.

Microdevice design and fabrication

The microdevice is composed of three main compartments: a hydrogel compartment for organoid culture in the centre, two basal side medium reservoirs flanking the hydrogel compartment, and inlet and outlet medium reservoirs for perfusion of the microchannel (see microdevice schematic structure in Fig. 1, Extended Data Fig. 1). A 1,200-µm-wide and 1,500-µm-long central hydrogel chamber is sandwiched by two open basal side medium reservoirs (4 mm in diameter), separated from the hydrogel chamber by phase-guiding features. The phase-guiding features consist of semi-walls shielding the hydrogel compartment 200 µm from the top combined with a row of pillars spanning the entire height. This design allowed liquid hydrogel loading without spillage to the basal side reservoirs, as well as enabling passive medium diffusion to the basal side of epithelial tissues and/or matrix-embedded cells. From the other sides, the hydrogel chamber was connected to a pair of inlet and outlet reservoirs for medium perfusion and an extra matrix-loading port through which the hydrogel was loaded. Inlet and outlet medium reservoirs, 1.5 mm in diameter, had a dual function: as apical medium reservoirs for perfusion of mini-gut lumens; and to facilitate injection of medium in small quantities for functional tests or bacterial co-culture and so on. Additional smaller ports were designed to allow the connection of perfusion pump tubings to the inlet and outlet reservoirs; in this case inlet and outlet reservoirs also function as air-bubble traps.

The microchip platform was fabricated using conventional soft-lithography methods established at the Center of Micronanotechnology (CMi, EPFL). In brief, the device was drawn using a CleWin (Phoenix Software). The designed layout was written with a diode laser with 2,000-nm resolution onto a fused silica plate coated with chrome and positive photoresist (Nanofilm) using an automated system (VPG200, Heidelberg Instruments). Exposed photoresist was removed with a developer (DV10, Süss MicroTec) and the chrome layer underneath was etched with an acid–oxidizer solution of perchloric acid, cerium ammonium nitrate and water. The resulting mask was developed with TechniStrip P1316 (Microchemicals) to remove the residual resist and extensively washed with ultra-pure water. The mould was made from multiple-layered epoxy-based negative photoresist SU8. First, a 200-µm thick layer of SU8 GM1075 (Gerlteltec) photoresist was cast onto a dehydrated silicon wafer using a negative resist coater (LMS200, Sawatec). The wafer was aligned and exposed to ultraviolet (UV) radiation through the first mask (MA6/BA6, Süss MicroTec). After baking at 95 °C, a second 200-µm thick layer of SU8 GM1075 was spin-coated, baked and exposed to UV through the second mask, carefully aligned using dedicated alignment marks. After the post-exposure bake, the wafer was developed with propylene glycol monomethyl ether acetate (Sigma) and baked at 135 °C for 4 h. The wafer was then plasma-activated and silanized with vapored trichloro (1*H*,1*H*,2*H*,2*H*-perfluorooctyl) silane (Sigma-Aldrich) overnight. This wafer was then used for polydimethylsiloxane (PDMS) moulding (Sylgard 184, Dow Corning). Ten weight-parts of elastomer base were vigorously mixed with 1 part of curing agent and poured onto the mould. After degassing under vacuum, PDMS was baked for 24 h at 80 °C. The resulting PDMS replica was cut and punched with appropriate size biopsy punchers. PDMS chips were soaked in a series of organic solvents to remove unreacted PDMS macromers. The resulting PDMS chips were exposed to oxygen plasma and irreversibly bonded on 35 mm glass bottom dishes (ibidi). Chips were sterilized with UV and kept sterile until further use.

Hydrogel loading and microchannel fabrication

An extracellular matrix mixture containing 75% (v/v) native bovine dermis type-I collagen solution (5 mg ml^{-1}, Koken, AteloCell) neutralized with 1 M sodium bicarbonate, 10× Dulbecco's modified Eagle's medium and Advanced DMEM/F12 (Gibco) to generate 4 mg ml^{-1} solution and 25% (v/v) Matrigel (Corning, growth-factor-reduced, phenol-red-free

formulation) was injected into the hydrogel compartment of the microdevice through the hydrogel-loading port and incubated at 37 °C for 2 min, after which inlet and outlet and basal side medium reservoirs were filled with Advanced DMEM/F12 medium supplemented with 1× Glutamax, 10 mM HEPES and 100 μg ml^{-1} penicillin–streptomycin (Gibco). The stiffness of the resulting polymerized hydrogel was consistent from batch to batch and remained at 750 ± 50 Pa. Generation of the microchannels within the hydrogel was performed using a nanosecond laser system (1-ns pulses, 100-Hz frequency, 355 nm; PALM MicroBeam laser microdissection system, Zeiss) equipped with a 10×/0.25 NA objective, at a constant stage speed and a laser power[35]. A pattern of consecutive parallel lines was created in Wolfram Mathematica and then imported into the PALM MicroBeam system's interface. Pattern was positioned along the microdevice matrix compartment, covering its entire length, 160 μm from the glass surface. Laser power and etching speed were adjusted to achieve 110–120 μm height microchannel in the hydrogel. After microchannel generation, the devices were perfused with Advanced DMEM/F12 medium, supplemented with 1× Glutamax, 10 mM HEPES and 100 μg ml^{-1} penicillin–streptomycin (Gibco), and maintained at 37 °C in 5% CO_2 humidified air.

Mini-gut development and culture

For mini-gut preparation, mouse intestinal organoids (between passage numbers 5 and 20) were dissociated into single cells. Organoids were removed from Matrigel, washed in BM (see medium formulations in 'Cell culture') and then dissociated with TrypLE express solution (Gibco) containing 2,000 U ml^{-1} DNaseI (Roche), 1mM *N*-acetylcysteine (Sigma-Aldrich) and 10 μM Y27632 (Stemgent) for 8 min at 37 °C. Dissociated cells were washed in BM, supplemented with 10% HI-FBS (Gibco) and passed through a 40-μm cell strainer. After centrifugation at 800*g* for 4 min, the pellet was resuspended in ENRCV medium containing 2.5 μM thiazovivin (Stemgent) (termed ENRCVT) at a density of about 10^6 cells per ml. After the removal of medium from the microchannel inlet, outlet and basal side medium reservoirs, 5 μl of cell suspension was introduced into the inlet and cells were allowed to fill the laser-ablated microchannel by gravity-driven flow. Cells were allowed to settle down in crypt-shaped cavities for about 3–6 min. All non-adherent cells were gently washed out from the microchannel by perfusion with ENRCVT. The medium reservoirs (inlet, outlet and basal side reservoirs) were filled with ENRCVT medium and the microdevice was incubated at 37 °C in 5% CO_2 humidified air. The medium was changed every day. After the completion of epithelial tube formation (typically 2–3 days) ENRCV medium in the inlet and outlet reservoirs was replaced with differentiation medium (ENR), lacking CHIR99021 and valproic acid, keeping expansion ENRCV medium in the basal side medium reservoirs for another few days. After tissue maturation (typically 4–6 days; depending on the starting number of cells loaded into the tube and the stem cell proliferation rate), the concentration of CHIR99021 and valproic acid (C and V) in the basal side medium reservoirs was gradually decreased over the next three days until complete removal of these growth factors from the medium. Dead cells accumulating in the lumen were removed, and medium changes in the microchannel were performed, either manually or automatically, by perfusing with fresh medium every 12 h. The medium in the basal side medium reservoirs was changed every 24 h. Of note, mini-gut tube growth during the first two weeks was found to be very robust and reproducible, with approximately 9 out of 10 tissues developing properly (that is, acquiring similar morphology, cell-type composition and pattern along a crypt–villus-like axis). Tissue defects and failure of proper mini-gut development, detected in around 10% of cases, may be caused by technical problems related to microdevice preparation (for example, defective microfluidic chips), hydrogel preparation or issues related to organoid culture. The reliable long-term (more than two weeks) culture of mini-guts critically depends on repeated perfusions and medium changes, as well as adequate microdevice handling. Overall, approximately 8 out of 10 mini-gut tubes could be successfully cultured for one month. A detailed protocol describing mini-gut development and culture has been deposited in the Protocol Exchange repository[28].

For macrophage mini-gut co-culture experiments, macrophages were resuspended in the ECM mixture (as described, 75% collagen/25% Matrigel (v/v)) and loaded into the hydrogel compartment of the microdevice. After hydrogel polymerization, BM supplemented with 50 ng ml^{-1} M-CSF (Sigma-Aldrich) was added to the inlet, outlet and basal side medium reservoirs. Laser ablation of the microchannel was performed using the described procedure. Macrophages were ablated in the microchannel region, but remained intact in the surrounding matrix. ISCs were seeded the next day, following the previously described protocol, and mini-guts co-cultured with macrophages were maintained in ENRWM medium (BMGF supplemented with growth factors (50 ng ml^{-1} EGF (Peprotech), 100 ng ml^{-1} Noggin (EPFL Protein Expression Core Facility), 500 ng ml^{-1} R-Spondin 1 (EPFL Protein Expression Core Facility), 50 ng ml^{-1} WNT3A (Time Bioscience) and 50 ng ml^{-1} M-CSF (Sigma-Aldrich)). Thiazovivin (2.5 μM) was added during the first 24 h to prevent apoptosis. After complete epithelium formation (2–3 days), ENRWM medium in the inlet and outlet reservoirs was replaced with differentiation medium (ENR). Over the next three days, the concentration of WNT3A in ENRWM medium in the basal side medium reservoirs was gradually decreased until complete removal from the medium. ENR and ENRM medium, in the inlet and outlet and the basal side medium reservoirs, respectively, was replenished every day. M-CSF was used in the basal side medium reservoirs to support the maintenance of macrophages.

For myofibroblast mini-gut co-culture experiments, mouse intestinal myofibroblasts (used between passages 3 and 8) were washed with PBS and dissociated with TrypLE Express solution (Gibco) for 5 min at 37 °C. Dissociated cells were passed through a 40-μm cell strainer, centrifuged at 800*g* for 4 min and resuspended at a density of about 10^5 cells per ml in DMEM supplemented with 10% HI-FBS, 1× L-glutamine, 1× non-essential amino acids solution, 1× insulin–transferrin–selenium, 100 μg ml^{-1} penicillin–streptomycin (Gibco) and 1× Primocin (Invivogen), termed MyoDMEM. After the removal of medium from the inlet, outlet and basal side medium reservoirs, 5 μl of cell suspension was introduced into the inlet and cells were allowed to fill in the laser-ablated microchannel by gravity-driven flow. Cells were allowed to settle in crypt-shaped cavities for about 5–10 min and all non-adherent cells were gently washed out from the microchannel and inlet and outlet reservoirs. All medium reservoirs were filled with MyoDMEM medium and the microdevice was incubated at 37 °C in 5% CO_2 humidified air. ISCs were co-seeded into mini-guts 3–4 h later, following the previously described protocol, and mini-guts co-cultured with myofibroblasts were maintained in ENRCVT medium supplemented with 5% HI-FBS.

For bile duct tubes, mouse ductal organoids were digested with TrypLE Express solution (Gibco) into single cells for 10 min at 37 °C. Digestion was stopped by adding BM containing 10% HI-FBS (Gibco) and cells were passed through a 40-μm cell strainer. Single cells were seeded in the microdevice at a density of 0.5 million cells per ml. Cells were allowed to settle for 10 min and excess cells were gently washed out from the microchannel. The bile duct tubes were cultured in expansion medium (EM) supplemented with Noggin and Y-27632 for one day, then the medium was changed to EM. After three days, the medium was replaced by cholangiocyte differentiation medium with modifications[36], BM supplemented with 1× B27 supplement, 1× N2 supplement (Gibco), 1.25 μM *N*-acetylcysteine (Sigma-Aldrich) and growth factors (50 ng ml^{-1} EGF (Peprotech), 50 ng ml^{-1} HGF (Peprotech), 0.1 μM dexamethasone (Sigma-Aldrich/Merck), 10 nM gastrin (Sigma-Aldrich) and 1.25 μM *N*-acetylcysteine (Sigma-Aldrich). The medium in both basal side medium reservoirs and the perfusion channel was changed every day.

For generating human mini-gut and mini-airway tubes, organoids were dissociated into single cells in TrypLE Express solution (Gibco)

for 15 min at 37 °C and seeded into the microdevices as described above for mouse ISCs. Non-adherent cells were washed away from the lumen and human mini-guts were subsequently cultured for the first two days in medium containing EGF, Noggin, R-Spondin, gastrin and Y-27632, and then switched to human ISC expansion medium as previously described. The medium for human mini-guts and mini-airway tubes was changed every day.

Human mini-airway tubes were cultured in airway organoid medium from day 0 onwards. At day 5, the medium in the inlet reservoirs was removed and an air–liquid interface culture established.

Human umbilical vein endothelial cells (HUVECs) (Lonza) were maintained in EGMTM-2 Bulletkit medium (Lonza) and used until passage 12. For 3D culture of endothelial tubes, cells were washed with PBS and then dissociated with TrypLE Express solution (Gibco) for 5 min at 37 °C. Dissociated cells were passed through a 40-µm cell strainer (Falcon), centrifuged at 1,000 rpm for 4 min and resuspended in EGMTM-2 medium at a density of 10^6 cells per ml. ECM mixture (as described previously, 75% collagen/25% Matrigel (v/v)) was prepared and loaded into the hydrogel compartment of the microdevice. The microchannel layout was adapted to mimic a blood-vessel-like bifurcation. Laser ablation was performed using standard parameters and cell suspension was added to the inlet and outlet reservoirs. After 5–10 min of incubation, inlet and outlet reservoirs were washed with EGMTM-2 and all reservoirs were filled with EGMTM-2 medium. Endothelial tubes were incubated at 37 °C in 5% CO_2 humidified air and medium was changed every day during the following two weeks of culture.

Immunofluorescence staining

Mini-guts were rinsed with PBS and fixed in 4% paraformaldehyde (PFA; ABCR) for 30 min at room temperature. After rinsing with PBS, samples were permeabilized with 0.2% Triton X-100 (Sigma-Aldrich) in PBS (1 h, room temperature) and blocked in 10% goat serum in PBS (Gibco) containing 0.01% Triton X-100 (termed blocking buffer) for at least 5 h or overnight. Samples were subsequently incubated overnight at 4 °C with primary antibodies diluted in blocking buffer. The following primary antibodies were used: lysozyme (1:50; Thermo Fisher Scientific, PA1-29680), Muc2 (1:50; Santa Cruz, sc-15334), chromogranin A (1:50; Santa Cruz, sc-13090), L-FABP (1:50; Santa Cruz, sc-50380), E-cadherin (1:50, Abcam, ab11512), SOX9 (1:50; Abcam, ab185966), Ki67 (1:50, BD Pharmingen, 550609), GP2 (1:50, MBL, D278-3), EpCAM (1:200, Thermo Fisher Scientific 17-5791-82, APC-conjugated) and ZO-1 (1:50, Thermo Fisher Scientific 33-9100). After washing with blocking buffer for at least 6 h, samples were incubated overnight at 4 °C with secondary antibodies Alexa Fluor 647 goat anti-rabbit, Alexa Fluor 546 goat anti-mouse, Alexa Fluor 488 goat anti-rat, Alexa Fluor 568 donkey anti-mouse, Alexa Fluor 647 donkey anti-rabbit (1:500, Invitrogen), Alexa Fluor 546 phalloidin and Alexa Fluor 488 phalloidin (1:40, Invitrogen) diluted in blocking buffer. Samples were extensively washed for at least 24 h before imaging. Proliferative cells were stained with a Click-iT EdU Alexa Fluor 647 imaging kit (Thermo Fisher Scientific) following the manufacturer's protocol.

Microscopy and image processing

Bright-field and fluorescent (eGFP, FITC–dextran) imaging of living mini-gut tubes was performed using a Nikon Eclipse Ti inverted microscope system equipped with a 4×/0.20 NA, 10×/0.30 NA and 20×/0.45 NA air objectives, 395-nm, 470-nm, 555-nm and 632-nm filters, DS-Qi2 and Andor iXon Ultra DU888U (Oxford Instruments) cameras and controlled by NIS-Elements AR 5.11.02 (Nikon Corporation) software. Fixed samples were imaged with a Zeiss LSM 700 Inverted Microscope (Bioimaging and Optics Core Facility), equipped with 10×/0.30 NA and 20×/0.80 NA air objectives, 405-nm, 488-nm, 555-nm and 639-nm lasers and controlled by ZEN 2010 imaging software (Zeiss). Image processing was mainly performed using ImageJ (NIH) using standard contrast and intensity level adjustments. Time-lapse images were acquired on Nikon Eclipse Ti inverted microscope and processed in ImageJ (NIH) using plug-ins for SIFT linear stack alignment, illumination correction, as well as custom-made scripts developed at EPFL's Bioimaging and Optics Core Facility. Extended depth of field (EDF) of bright-field images was calculated using built-in NIS-Elements function for a *z*-stack of 80–100 µm. Animated Supplementary Videos were rendered using Imaris (Bitplane), ImageJ (NIH) and Premiere Pro (Adobe).

Histology

Samples were prepared by the Histology Core Facility (EPFL) in accordance with standard procedures. The hydrogel compartment was cut around its perimeter using a razor blade, which allowed us to extract a block of hydrogel containing mini-gut tubes. The samples were fixed in 4% PFA for 12 h at room temperature, washed in 1× PBS and cryoprotected in 1 M (or 30%) sucrose overnight at 4 °C. The samples were equilibrated for 1 h in 7.5% gelatin solution in 1 M sucrose/0.12 M phosphate buffer at 37 °C, placed in a mould filled with gelatin and frozen in cold isopentane (−70 °C). Sectioning was done using a Leica cryostat CM3050S at −30 °C. Section thickness was set at 8 µm. For staining, sections were hydrated in distilled water and immersed in Alcian Blue pH 2.5 solution for 25 min, counterstained with Nuclear Fast Red, dehydrated and mounted with a xylene-based glue. Sections were imaged on a LEICA DM 5500 microscope, DMC 2900 colour camera. Image processing was performed using ImageJ (NIH) using standard contrast and intensity level adjustments.

TEM, sample preparation and imaging

Microfluidic chips were cut around the hydrogel compartment. Blocks of hydrogel containing epithelial tubes were extracted from the chips and chemically fixed in a mix of 2.5 % glutaraldehyde and 2.0 % PFA in 0.1 M phosphate buffer (pH 7.4) and left for 4 h. Hydrogel blocks were trimmed with a razor blade to ensure that they were not larger than approximately 1 mm along one of the axes. The samples were washed thoroughly with cacodylate buffer (0.1 M, pH 7.4), post-fixed for 40 min in 1.0 % osmium tetroxide with 1.5 % potassium ferrocyanide, and then for 40 min in 1.0 % osmium tetroxide alone. The samples were stained for 30 min in 1% uranyl acetate in water before being dehydrated through increasing concentrations of alcohol and then embedded in Durcupan ACM (Fluka) resin. The samples were then placed in moulds and the resin polymerized at 65 °C for 24 h. Sections (50-nm thickness) were cut with a diamond knife, and collected onto single-slot copper grids with a pioloform support film. Sections were contrasted with lead citrate and uranyl acetate, and images were taken with a transmission electron microscope at 80 kV (Tecnai Spirit, FEI with Eagle CCD camera). Image processing was performed using ImageJ (NIH) using standard contrast and intensity level adjustments.

Measurement of aminopeptidase activity

For measurements of the specific activity of the apical brush border aminopeptidase, mini-guts were disconnected from the microfluidic syringe pump. The inlet reservoir was manually filled with 1.5 mM L-alanine-4- nitroanilide hydrochloride (A4N; Sigma-Aldrich) solution in ENR medium and allowed to flow through the lumen to the outlet reservoir. After 1 h incubation at 37 °C, the medium was collected from the outlet reservoir. Cleavage product (4-nitroaniline) was quantified using a NanoDrop spectrophotometer (Thermo Fisher Scientific) at 405 nm using ENR medium as a reference. Enzymatic activity was quantified based on the average, measured for $n = 3$ biologically independent samples.

scRNA-seq

The cDNA library was constructed using 10X genomics Chromium 3′ reagents v.3, and sequenced using Illumina protocol 15048776 using NextSeq v.2.5 reagents, with a read length of 52 nucleotides and around 70,000 reads per cell. The reads were aligned to mm10 with

Cell Ranger v.3.0.1. Raw count matrices were imported in Seurat 2.3.4 (ref. [37]) using RStudio 1.1.463 (www.rstudio.com), and single live cells were selected on the basis of the number of detected genes (approximately 2,500–5,000) and fraction of mitochondrial genes (around 0.05–0.15). The number of cells after filtering was 998 (for organoids), 961 ('young' mini-guts), 1,000 ('old' mini-guts) and 611 (mini-guts infected with *C. parvum*). The data were normalized to 10,000 counts per cell, and log1p-transformed using the natural logarithm (referred to as log(expression)). The four datasets were aligned using Seurat canonical correlation analysis on the intersection of the most variable genes, and dimensionality reduction was conducted with UMAP[38] in the aligned correlated component space. Louvain clustering yielded 40 clusters that were merged and named on the basis of canonical cell type markers. Cell-cycle scoring was based on published signatures[39], and cells in the G2/M phases, which had a gene signature predominantly associated with cell division, were referred to as 'dividing cells'. Gene sets highlighting villus-top enterocytes[13], M cells[9] and enteroendocrine cells[38] were taken from the respective literature. A similar clustering analysis was performed on the dataset GSE92332 from a previous study[9], designated as 'atlas', to obtain a reference of the approximate proportions of in vivo cell types. The datasets from mice B2 to B10 were used, whereas B1 was excluded because of strong technical differences to the others. The original cell-type annotations from the atlas were merged to fit our simplified naming: enterocyte immature distal, enterocyte immature proximal, enterocyte mature distal, enterocyte mature proximal, enterocyte progenitor and enterocyte progenitor late were referred to as 'enterocytes'; stem, transit amplifying (TA) early and TA G1 were referred to as 'stem and progenitor cells'; TA G2 and enterocyte progenitor early corresponded to dividing cells. The annotations for other cell types (Paneth, goblet, enteroendocrine and Tuft cells) already corresponded to our respective clusters. Visual representations of the data were generated using Seurat internal functions or ggplot2[40] and cosmetic adjustments were made in Adobe Illustrator. Simultaneous displays of several markers were generated from subtractive colour overlay. Gene set enrichment analysis (GSEA) was performed using the Broad Institute Java stand-alone application v.3.0, with single cells exported to each be considered as a stand-alone RNA-seq dataset associated to both a cell type and a treatment condition. The hallmark gene sets from MSigDB[41] were scored across conditions either for all cell types as a bulk, or cell type by cell type, using signal to noise as a metric and the 'classical' enrichment statistic, and estimated the family-wise error-rate *P* values were empirically estimated based on 10,000 random phenotype permutations.

The following algorithm was applied to define the best cell-type markers: (1) ribosomal proteins and genes with less than 25% dropout rate were excluded, because genes that are ubiquitously expressed or large families of closely related highly expressed proteins are not useful cell-type-specific biomarkers. (2) The gene expression from cells in each cluster was compared pairwise to that from cells in each other cluster by using the Wilcoxon rank-sum test. Only positive markers were considered. The highest *P* value and lowest average log ratio from the pairwise comparisons were kept as being the *P* value and log ratio for each gene in each cluster. (3) The following exceptions were made to the previous rule: (i) the cluster of dividing cells was not used in the pairwise comparisons when looking for markers for the other clusters, because dividing cells might display some markers from any cell type, especially progenitors. (ii) When looking for stem and progenitor cell markers, we further excluded Paneth cells from the pairwise comparisons, because Paneth cells are also expected to be positive for many canonical crypt and stem cell markers. (iii) When looking for enterocyte markers, we excluded 'top enterocytes' from the pairwise comparisons, because these cells are expected to express enterocyte markers. (iv) Paneth cells were excluded from the pairwise comparisons when looking for goblet cell markers, as some of the most commonly used goblet cell markers are secretory cell markers that are also expressed in Paneth cells. (4) To define 'markers', we applied a filtering with a double cut-off on significance and log ratio: worst *P* value in pairwise comparisons less than 0.05, and worst log ratio higher than 1.25 (that is, ratio more than 3.5). The complete list is shown in the Source Data for Extended Data Fig. 5. (5) We defined the 'best markers' as the top markers when sorting by descending log ratio. The lists of best markers were used to generate the heat maps, in which the unscaled log(expression) of these genes was plotted against cells grouped by cell type, and sorted by UMAP coordinates within each cluster to facilitate visualization of gradients along the ISC-to-enterocyte axis. A Wilcoxon signed-rank test was used to compute the *P* values reported for volcano plots (across datasets, as a bulk or by cell type).

To align the in vivo atlas to our in vitro datasets, we converted the two Seurat v.2 objects containing the four in vitro datasets and nine in vivo datasets, respectively, to Seurat v.3, and applied Harmony v.1.0 (ref. [42]) alignment across modalities and across datasets. The alignment and dimensionality reductions were based on 30 dimensions. The result is shown as a UMAP in the Harmony-aligned space. For more information or complete reproduction, see 'Data availability' and 'Code availability'.

Modelling intestinal epithelial damage and regeneration

Mini-guts and intestinal organoids were treated with DSS (MP Biomedicals) to induce epithelial damage. DSS (0.05%) in ENR medium was administered through the inlet reservoir to perfuse the lumen of 7-day-old mini-guts and added to the wells with organoids on day 3 after passaging. After DSS treatment for 24 h, the medium was changed to ENR without DSS, and mini-gut tubes were further cultured for 12 days according to standard protocols. Organoids, collapsed in response to DSS, were carefully collected, washed, re-embedded in fresh Matrigel and cultured in expansion medium (ENRCV). Similar results were obtained in at least three independent experiments with three replicates.

For irradiation experiments, mini-guts were exposed to 2-Gy and 8-Gy doses of gamma-radiation using Gammacell 1000 Elite 137Cs source (MDS Nordion) at 0,143 Gy s^{-1}. After irradiation, samples were cultured according to standard protocols and recovery was monitored for up to 11 days. Relative LGR5–eGFP fluorescence was quantified using a specialized ImageJ plug-in for separate crypt regions, normalized to the ROI area and then normalized background intensity was subtracted. Experiments were repeated independently at least twice with three replicates per each condition with similar results.

Rectangular gaps in the epithelium were generated using a nanosecond laser system (1-ns pulses, 100-Hz frequency, 355 nm; PALM MicroBeam (Zeiss) laser microdissection system) equipped with a 10×/0.25 NA objective, at a constant stage speed and a laser power. A pattern of consecutive parallel lines was positioned 20 µm above the bottom epithelium of the lumen. Laser power and etching speed were adjusted to induce cellular damage without ablation of the hydrogel. After epithelial tissue damage, samples were connected back to the automated syringe pump and perfused every 3 h, 0.25 µl per min for 20 min. Similar results were obtained in at least three independent experiments with three replicates.

Infection of mini-guts with *C. parvum*

C. parvum oocysts (Iowa strain, University of Arizona) were stored in sterile PBS with 100 µg ml^{-1} penicillin–streptomycin (Gibco) at 4 °C and used within two months. For mini-gut infection, around 1×10^6 oocysts were incubated in 10% (v/v) Clorox bleach in PBS on ice and washed three times with 1 ml BM medium and centrifugation (3 min, 8,000*g*, 4 °C). The oocysts were resuspended in 200 µl ENR medium supplemented with 0.5% (w/v) sodium taurocholate (Sigma-Aldrich). For mini-gut infection, a 5-µl suspension of oocysts was added directly to the inlet reservoir of the chip and left without perfusion for 6 h. Samples were perfused manually, in which 10 µl of medium was collected from the outlet reservoir and fresh ENR medium was added to the

inlet reservoir. In the following days, mini-guts were cultured as previously described, and perfusion was done manually twice a day. Media collected from infected mini-guts at different time points were pooled together and used for the detection of mouse inflammatory cytokines using a Multi-Analyte ELISArray kit (Qiagen, MEM-004A), following the manufacturer's protocol. The plotted values were normalized to the ENR medium used for mini-gut perfusion. Samples were imaged every day before perfusion on a Nikon Eclipse Ti-E microscope equipped with DS-Qi2 camera and 10×, 20× and 63× objectives. For immunofluorescence analysis, mini-guts were processed as described. After staining with DAPI and secondary antibodies, samples were washed three times, and fluorescein-labelled antibodies Crypt-a-Glo or Sporo-Glo (Waterborne) were added to label oocysts or intracellular stages of the parasite, respectively, and incubated at room temperature for 1 h. After washing once with 0.1% Tween-20 in PBS, the samples were imaged on s Leica SP8 confocal microscope (Bioimaging and Optics Core Facility), using LAS X software (Leica) and processed using standard contrast and intensity level adjustments in ImageJ (NIH).

In another set of experiments aimed at assessing whether newborn oocysts could be obtained, mini-guts were infected with the sporozoites. As previously described, about 1×10^6 oocysts were incubated in 10 % (v/v) Clorox bleach in PBS on ice and washed three times with 1 ml BM medium by centrifugation (3 min, 8,000*g*, 4 °C). Oocysts were resuspended in 1 ml of freshly prepared excystation medium with 1.5% (w/v) sodium taurocholate (Sigma-Aldrich) in BM and incubated for 1.5 h at 37 °C. Samples were checked microscopically for the extent of excystation and then incubated for an additional 30 min to reach approximately 60–80% excystation. After incubation 9 ml of BM was added to remove remaining oocysts and shells, the suspension was filtered through a Swinnex-25 47-mm (Millipore) apparatus with a 3-µm pore-size polycarbonate filter (Costar/Nucleopore). Another 5 ml of DMEM was added to wash the filter and then the filtered sporozoite suspension was centrifuged for 20 min at 3,400*g* to pellet sporozoites. The sporozoites were resuspended in 200 µl of ENR and 5 µl was added directly to the inlet reservoirs of the chips and left without perfusion for 12 h. In the following days, mini-guts were perfused once a day and all medium was collected from the lumen for immunostaining to Crypt-a-Glo and DAPI. Samples were fixed in 4% PFA and centrifuged for 3 min at 8,000*g*. The pellet was washed twice in PBS and centrifuged for 3 min at 8,000*g*. The last time pellet was resuspended in 50 µl of Crypt-a-Glo containing 1 µg ml^{-1} DAPI. After 2 h of incubation at room temperature, samples were washed twice in PBS and centrifuged for 3 min at 8,000*g*. Finally, pellets were resuspended in 10 µl of PBS, transferred to glass-bottomed 24-well plates (MatTek) and left overnight at 4 °C before imaging to allow all oocysts to homogeneously sediment on the glass-bottom surface. Imaging was done on Zeiss LSM 700 Inverted Microscope (Bioimaging and Optics Core Facility), equipped with 10×/0.30 NA and 20×/0.80 NA air objectives and controlled by ZEN 2010 imaging software (Zeiss). Quantification was performed using the standard toolkit from ImageJ. Of note, presumably owing to an incomplete filtration process, some remaining oocyst and broken shells were observed at days 1–3. The experiment was designed in such a way that all medium from the lumen was collected during perfusion, leaving a minimal number of unattached oocysts and sporozoites in the mini-guts.

Electron microscopy of the *C.-parvum*-infected samples

For TEM, samples were fixed at day 1, 2, 3 and 5 and were processed as previously described[43]. In brief, the samples were fixed in 1% PFA and 2.5% glutaraldehyde in 0.1 M PB buffer for 2 h at room temperature, followed by 1 h incubation in 2% (w/v) osmium tetroxide and 1.5% (w/v) $K_4[Fe(CN)_6]$ in 100 mM PB buffer. Samples were incubated for 1 h in 1% (w/v) tannic acid in 100 mM PB buffer, then 30 min in 2% (w/v) aqueous solution of osmium tetroxide followed by 1% (w/v) uranyl acetate for 2 h at room temperature. At the end of gradual dehydration cycles, samples were flat-embedded in Epon-Araldite mix[43]. Polymerized flat blocks were trimmed using a 90° diamond trim tool, and the arrays of 100-nm sections were obtained using a 35° ATC diamond knife (Diatome) mounted on a Leica UC6 microtome. Sections were transferred to wafers using a modified array tomography procedure[44]. For the ultrastructure analysis, wafers were mounted on aluminium stubs and analysed using a FEI Helios Nanolab 650 scanning electron microscope (Thermo Fisher Scientific). The imaging settings were as follows: MD or ICD detectors, accelerating voltage: 2 kV, current 0.8 nA, dwell time 6 µs. Images were collected manually or using the AT module of the MAPS program (Thermo Fisher Scientific).

Reporting summary

Further information on research design is available in the Nature Research Reporting Summary linked to this paper.

Data availability

scRNA-seq data have been deposited to the Gene Expression Omnibus (GEO) public repository with the accession code GSE148366. Additional supporting data related to gene-expression analyses of mini-gut tubes infected with *C. parvum* have been deposited to https://figshare.com/projects/mini-guts/80819. Source data are provided with this paper.

Code availability

The code used for scRNA-seq data analysis is available at https://github.com/nbroguiere/miniguts.

28. Nikolaev, M. et al. Bioengineering microfluidic organoids-on-a-chip. *Protoc. Exch*. https://doi.org/10.21203/rs.3.pex-903/v1 (2020).
29. Koliaraki, V. & Kollias, G. Isolation of intestinal mesenchymal cells from adult mice. *Bio-protocol* **6**, e1940 (2016).
30. Huch, M. et al. In vitro expansion of single Lgr5$^+$ liver stem cells induced by Wnt-driven regeneration. *Nature* **494**, 247–250 (2013).
31. Takata, K. et al. Induced-pluripotent-stem-cell-derived primitive macrophages provide a platform for modeling tissue-resident macrophage differentiation and function. *Immunity* **47**, 183–198 (2017).
32. Blokzijl, F. et al. Tissue-specific mutation accumulation in human adult stem cells during life. *Nature* **538**, 260–264 (2016).
33. Miyoshi, H. & Stappenbeck, T. S. In vitro expansion and genetic modification of gastrointestinal stem cells in spheroid culture. *Nat. Protocols* **8**, 2471–2482 (2013).
34. Sachs, N. et al. Long-term expanding human airway organoids for disease modeling. *EMBO J*. **38**, e100300 (2019).
35. Brandenberg, N. & Lutolf, M. P. In situ patterning of microfluidic networks in 3D cell-laden hydrogels. *Adv. Mater*. **28**, 7450–7456 (2016).
36. Chen, C. et al. Bioengineered bile ducts recapitulate key cholangiocyte functions. *Biofabrication* **10**, 034103 (2018).
37. Butler, A., Hoffman, P., Smibert, P., Papalexi, E. & Satija, R. Integrating single-cell transcriptomic data across different conditions, technologies, and species. *Nat. Biotechnol*. **36**, 411–420 (2018).
38. Becht, E. et al. Dimensionality reduction for visualizing single-cell data using UMAP. *Nat. Biotechnol*. **37**, 38–44 (2019).
39. Kowalczyk, M. S. et al. Single-cell RNA-seq reveals changes in cell cycle and differentiation programs upon aging of hematopoietic stem cells. *Genome Res*. **25**, 1860–1872 (2015).
40. Wickham, H. *ggplot2: Elegant Graphics for Data Analysis* (Springer, 2016).
41. Subramanian, A. et al. Gene set enrichment analysis: a knowledge-based approach for interpreting genome-wide expression profiles. *Proc. Natl Acad. Sci. USA* **102**, 15545–15550 (2005).
42. Korsunsky, I. et al. Fast, sensitive and accurate integration of single-cell data with Harmony. *Nat. Methods* **16**, 1289–1296 (2019).
43. Kolotuev, I. Positional correlative anatomy of invertebrate model organisms increases efficiency of TEM data production. *Microsc. Microanal*. **20**, 1392–1403 (2014).
44. Burel, A. et al. A targeted 3D EM and correlative microscopy method using SEM array tomography. *Development* **145**, dev160879 (2018).
45. Mabbott, N. A., Donaldson, D. S., Ohno, H., Williams, I. R. & Mahajan, A. Microfold (M) cells: important immunosurveillance posts in the intestinal epithelium. *Mucosal Immunol*. **6**, 666–677 (2013).
46. Nakato, G. et al. New approach for M-cell-specific molecules screening by comprehensive transcriptome analysis. *DNA Res*. **16**, 227–235 (2009).
47. Hartl, M. & Schneider, R. A unique family of neuronal signaling proteins implicated in oncogenesis and tumor suppression. *Front. Oncol*. **9**, 289 (2019).
48. Funda, D. P. et al. CD14 is expressed and released as soluble CD14 by human intestinal epithelial cells in vitro: lipopolysaccharide activation of epithelial cells revisited. *Infect. Immun*. **69**, 3772–3781 (2001).

49. Nakamura, Y., Kimura, S. & Hase, K. M cell-dependent antigen uptake on follicle-associated epithelium for mucosal immune surveillance. *Inflamm. Regen*. **38**, 15 (2018).
50. Hase, K. et al. Distinct gene expression profiles characterize cellular phenotypes of follicle-associated epithelium and M cells. *DNA Res*. **12**, 127–137 (2005).
51. Dillon, A. & Lo, D. D. M cells: intelligent engineering of mucosal immune surveillance. *Front. Immunol*. **10**, 1499 (2019).
52. Lim, J. S. et al. Caveolae-mediated entry of *Salmonella typhimurium* in a human M-cell model. *Biochem. Biophys. Res. Commun*. **390**, 1322–1327 (2009).
53. Terahara, K. et al. Comprehensive gene expression profiling of Peyer's patch M cells, villous M-like cells, and intestinal epithelial cells. *J. Immunol*. **180**, 7840–7846 (2008).
54. Hase, K. et al. The membrane-bound chemokine CXCL16 expressed on follicle-associated epithelium and M cells mediates lympho-epithelial interaction in GALT. *J. Immunol*. **176**, 43–51 (2006).
55. Kanaya, T. & Ohno, H. The mechanisms of M-cell differentiation. *Biosci. Microbiota Food Health* **33**, 91–97 (2014).
56. Roulis, M. et al. Paracrine orchestration of intestinal tumorigenesis by a mesenchymal niche. *Nature* **580**, 524–529 (2020).

Acknowledgements We thank M. Juhas for the generation of stem-cell-derived macrophages and help with co-culture experiments; R. Guiet and O. Burri for programming image-processing plug-ins; J. Dorsaz, J. Pernollet and all engineers of the Center of Micronanotechnology (CMi, EPFL) for support in microfabrication; S. Rezakhani, G. Sorrentino and K. Schoonjans for help with cholangiocyte isolation; D. Schaefer and M. Riggs for providing oocysts; R. O'Connor for expertise in analysing *C. parvum* epicellular stages; F. Gorostidi and S. Kishore for providing trachea tissue samples; and A. Manfrin, S. Höhnel, G. Rossi, M. Knobloch and A. Persat for inputs on the manuscript. We acknowledge support from the following EPFL core facilities: CMi, Histology, BIOP, CryoEM and CECF. This work was funded by the Swiss National Science Foundation (SNSF) research grant 310030_179447; the National Center of Competence in Research (NCCR) 'Bio-Inspired Materials' (https://www.bioinspired-materials.ch/); the EU Horizon 2020 research programme INTENS (http://www.intens.info/); the Personalized Health and Related Technologies (PHRT) Initiative from the ETH Board; and EPFL. S.G. was supported in part by a fellowship from the Novartis Foundation for Medical-Biological Research. N.G. was supported in part by an EMBO Long-Term Postdoctoral Fellowship.

Author contributions M.N. and M.P.L. conceived the study, designed experiments, analysed data and wrote the manuscript. N. Broguiere analysed all scRNA-seq data. S.G. developed an early version of the organoid culture technology and contributed to study design. M.N. and Y.T. designed the microdevice. M.N and O.M. conducted experiments on modelling damage and regeneration. O.M. performed human mini-gut and airway tube experiments. M.N. and D.D. performed and analysed *C. parvum* infection experiments. I.K. performed electron microscopy imaging of the *C.-parvum*-infected samples. B.E. performed bile duct tube experiments. N. Brandenberg and N.G. conducted preliminary experiments on matrix microstructuring and contributed to study design. H.C. proposed and designed *C. parvum* infection experiments and provided feedback on the manuscript.

Competing interests The EPFL has filed for patent protection (EP16199677.2, PCT/EP2017/079651, US20190367872A1) on the scaffold-guided organoid technology described herein, and M.P.L., M.N., S.G., Y.T., N. Brandenberg and N.G. are named as inventors on those patents. M.P.L. and N. Brandenberg are shareholders in SUN bioscience SA, which is commercializing those patents. H.C. is an inventor on several patents related to organoid technology. The other authors declare no competing interests.

Additional information

Supplementary information is available for this paper at https://doi.org/10.1038/s41586-020-2724-8.

Correspondence and requests for materials should be addressed to M.P.L.

Peer review information *Nature* thanks Dominic Grun, Thomas F. Meyer, Honorine Ward and the other, anonymous, reviewer(s) for their contribution to the peer review of this work.

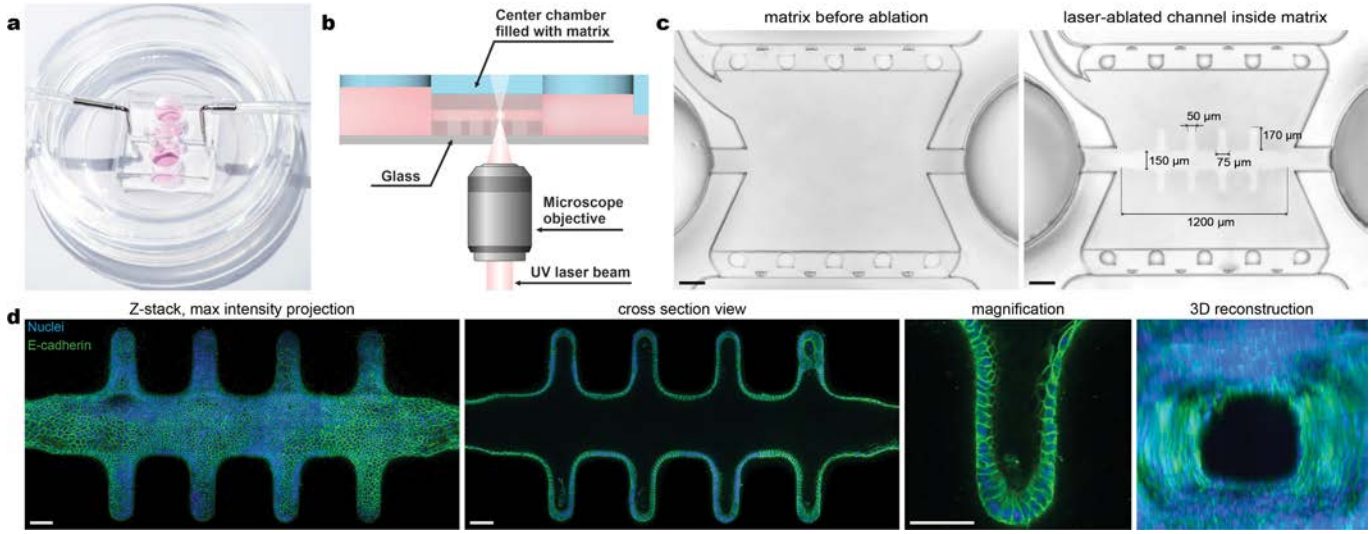

Extended Data Fig. 1 | Bioengineering intestinal stem cell epithelia with a tubular, in-vivo-like architecture. a, Photograph of the fully assembled microchip system. **b**, Schematic cross-sectional view of laser ablation using a nanosecond-pulsed laser. **c**, Hybrid collagen I/Matrigel scaffold in the central chamber before and after microchannel ablation. Scale bars, 200 µm. **d**, Fluorescence confocal images of a representative three-day old epithelial tube. Cells are labelled with DAPI (blue, nuclei) and E-cadherin (green). Images correspond to the maximal intensity projection of a *z*-stack of 100 µm. Scale bars, 50 µm. Data are representative of at least two independent experiments.

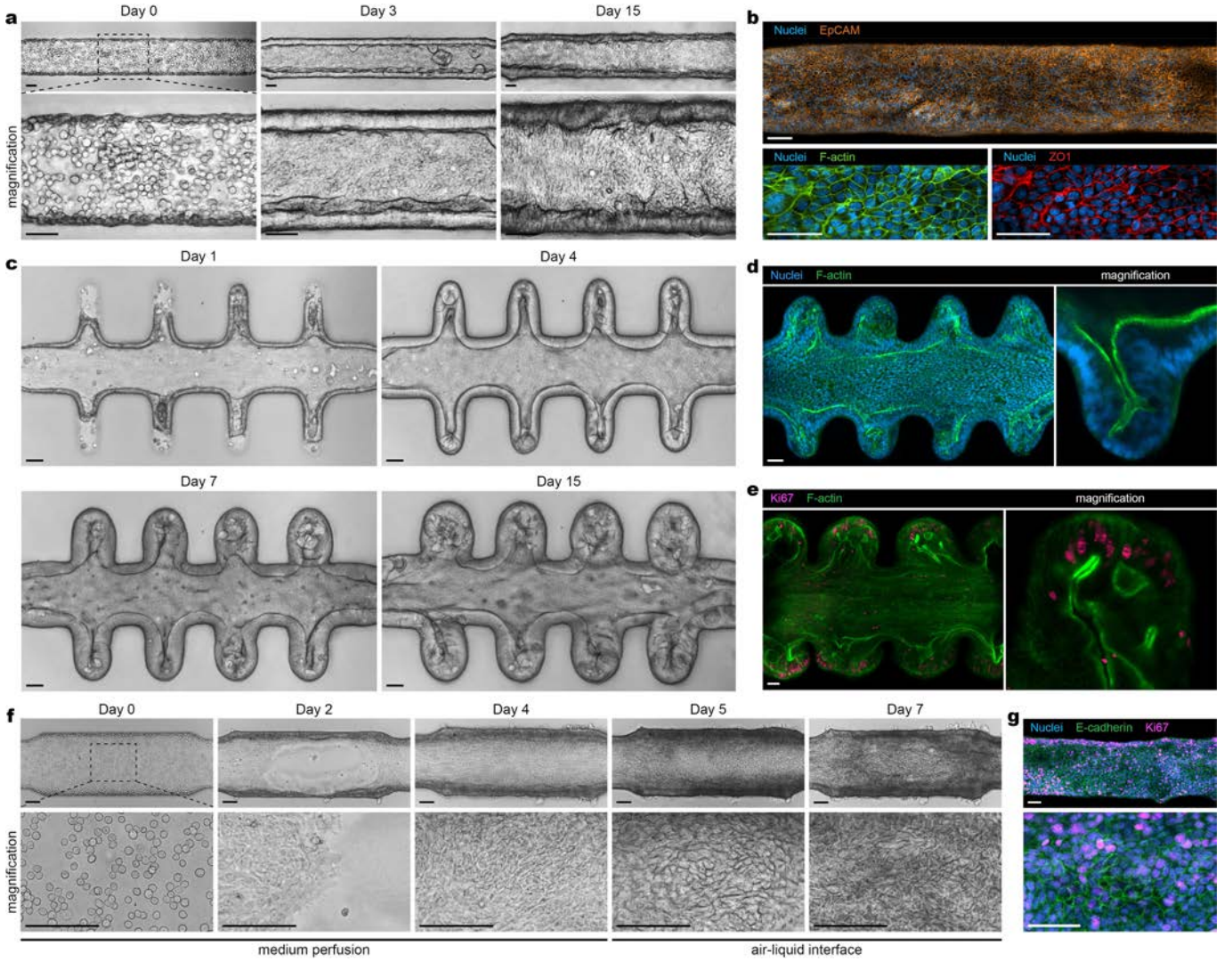

Extended Data Fig. 2 | Establishment of shape-controlled organoid culture from a variety of epithelial stem and progenitor cells. a, Development of bile duct tube composed of mouse cholangiocytes. **b**, Fluorescence confocal images of representative 3-day-old bile duct tubes, showing an entire tissue (top) stained for EpCAM (orange) and a higher magnification view (bottom) stained for actin filaments (green) and tight junction protein ZO-1 (red). Nuclei stained with DAPI (blue). Scale bars, 50 µm. **c**, Development of tubular mini-guts composed of human ISCs. **d**, Fluorescent confocal image showing formation of tightly packed single-layered epithelium in 15-day-old human mini-gut. **e**, Fluorescent confocal image showing proliferating Ki67^{+} cells predominantly localized to the crypts in 10-day-old human mini-gut. Nuclei and actin filaments stained with DAPI (blue) and Phalloidin (green), respectively. Images correspond to the maximal intensity projection of a *z*-stack of 80 µm. **f**, Formation of a human mini-airway epithelial tube and establishment of air–liquid interface (ALI) culture from day 5 onwards. Scale bars, 100 µm. **g**, Fluorescence confocal image of a representative 7-day-old human mini-airway epithelial tube, showing an entire tissue (top) and a higher magnification view (bottom) stained for nuclei (DAPI, blue), E-cadherin (green) and Ki67^{+} proliferating cells (pink). Scale bars, 50 µm. All data are representative of at least two independent experiments.

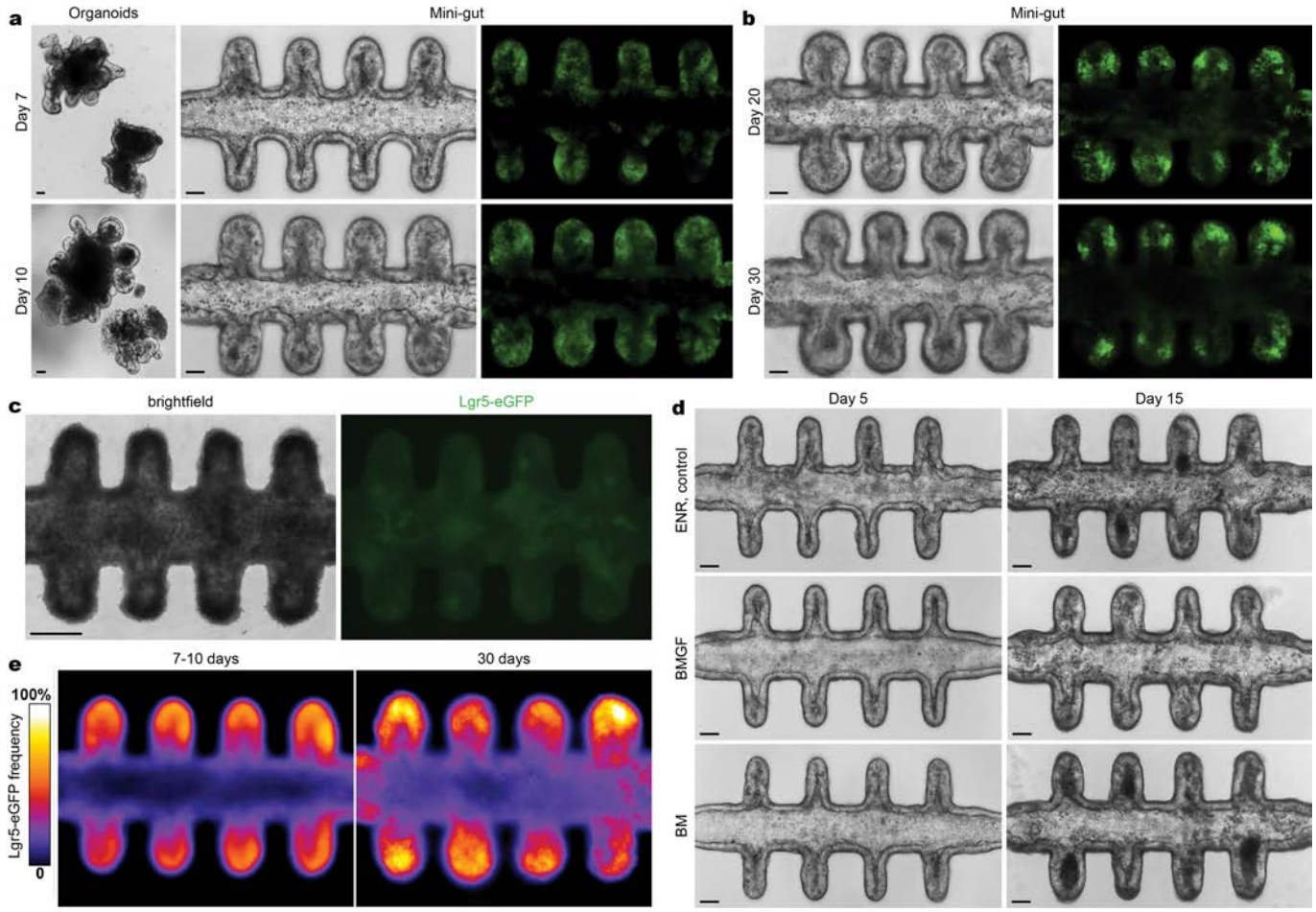

Extended Data Fig. 3 | Establishment of long-term culture and in vitro tissue homeostasis. a, Bright-field (middle) and LGR5–eGFP fluorescence (right) images of mini-gut progression on days 7 and 10, compared to organoids (left). **b**, Long-term propagation of mini-guts (up to 30 days) shown in bright-field (left) and LGR5–eGFP fluorescence (right). Data are represent ative of at least four independent experiments. EDF of bright-field images, calculated for a *z*-stack of 80 µm; fluorescence confocal images correspond to a maximal intensity projection of a *z*-stack of around 60 µm. Scale bars, 50 µm. **c**, Bright-field and LGR5–eGFP fluorescence of mini-gut deterioration due to the massive accumulation of dead cells within the lumen in the absence of perfusion. Scale bars, 100 µm. **d**, Tubular mini-guts maintain epithelial integrity and morphology in different cell culture media used for lumina perfusion. No difference in epithelium morphology and stability was detected when tissues were apically exposed to organoid culture medium (ENR) or minimal media lacking growth factors (BMGF, BM). Similar results were obtained in at least two independent experiments with $n = 2$ samples per each condition. Scale bars, 50 µm. **e**, Frequency map showing the localization of LGR5–eGFP-expressing ISCs in 7-10-day-old tissues (left) and 30-day-old tissues (right). Average of the maximal intensity projection of a *z*-stack of around 60 µm for $n = 20$ tissues (7–10-day-old) and $n = 8$ tissues (30-day-old).

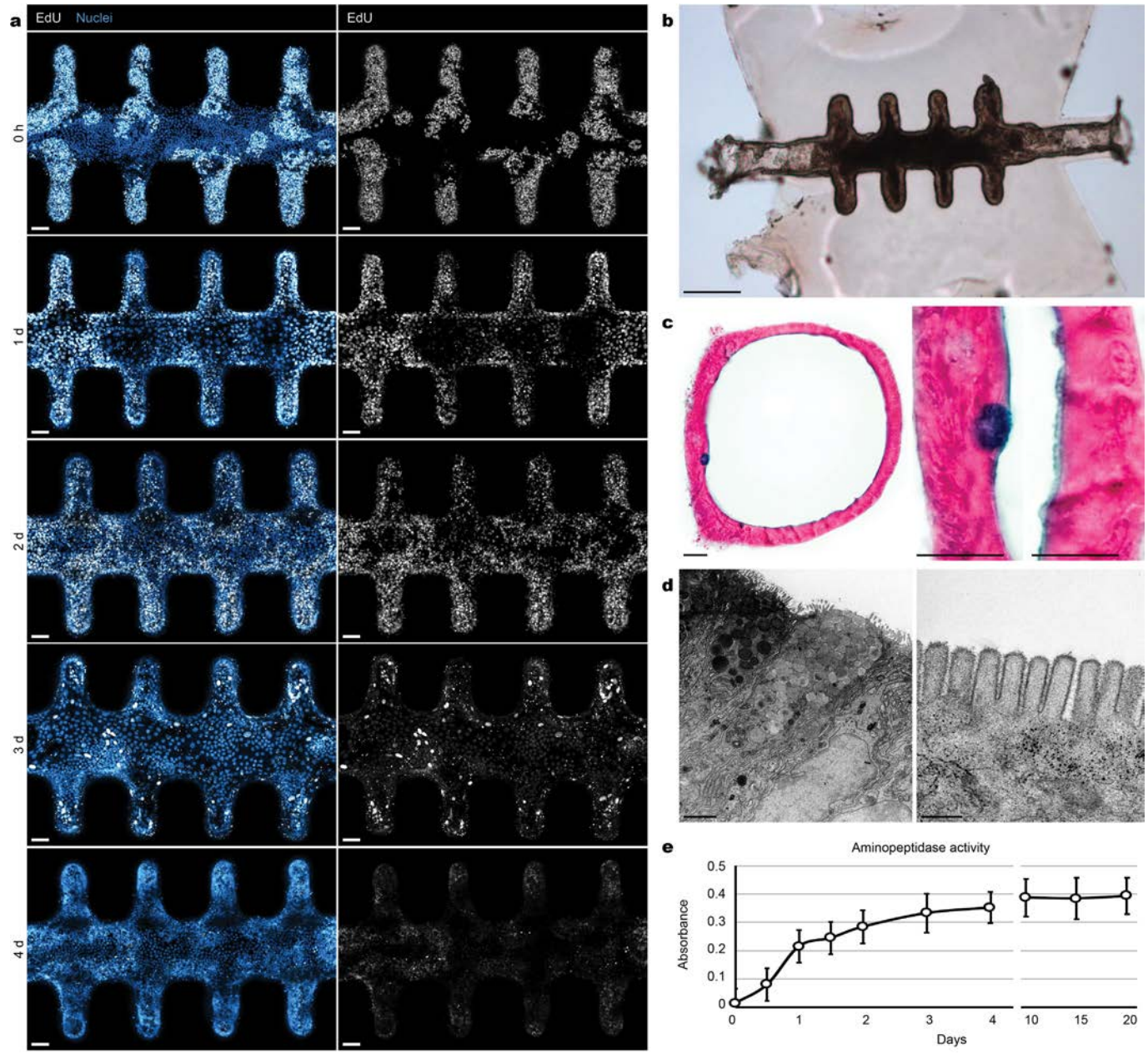

Extended Data Fig. 4 | Mini-gut tubes undergo rapid cell turnover and comprise key functional intestinal cell types. a, Epithelial tissue turnover assessed through EdU pulse-chase experiments. Ten-day-old mini-guts were treated with EdU for 12 h basally and apically, followed by a chase period of four days. At 0 h after EdU removal, the majority of EdU^+ cells resided within the crypts and adjacent regions. A 24-h EdU pulse-chase revealed distinct regions of cell proliferation that were to a large extent restricted to the crypts. Two days after the EdU pulse, numerous EdU^+ cells were found in the lumen, suggesting the occurrence of intestinal epithelial cell migration from the crypts to the villus-like domains. Labelled cells were virtually absent four days after the EdU pulse, suggesting that tubular mini-guts underwent full turnover of the epithelium. Data are representative of one EdU labelling experiment with $n = 2$ replicates per condition. Scale bars, 50 µm. **b**, Micrograph of a mini-gut tube removed from the microchip for downstream histological sectioning and analysis. Scale bar, 200 µm. **c**, Histological cross-sections of 7-day-old mini-gut tubes stained with Alcian Blue showing acidic polysaccharides of the mucus layer (blue) counterstained with Nuclear Fast Red. The entire perpendicular section (left) and a higher magnification view of the goblet cells (right) are shown. Similar results were obtained for 10 sections from two biologically independent samples. Scale bars, 20 µm. **d**, Transmission electron microscopy cross-sectional views of 7-day-old mini-gut tube. Goblet cell (left; scale bar, 2 µm) and enterocyte brush border (right; scale bar, 0.3 µm). Data are representative of two samples. **e**, Gradual increase in aminopeptidase activity after induction of differentiation in mini-gut tubes. Mean ± s.d. from $n = 3$ biologically independent experiments.

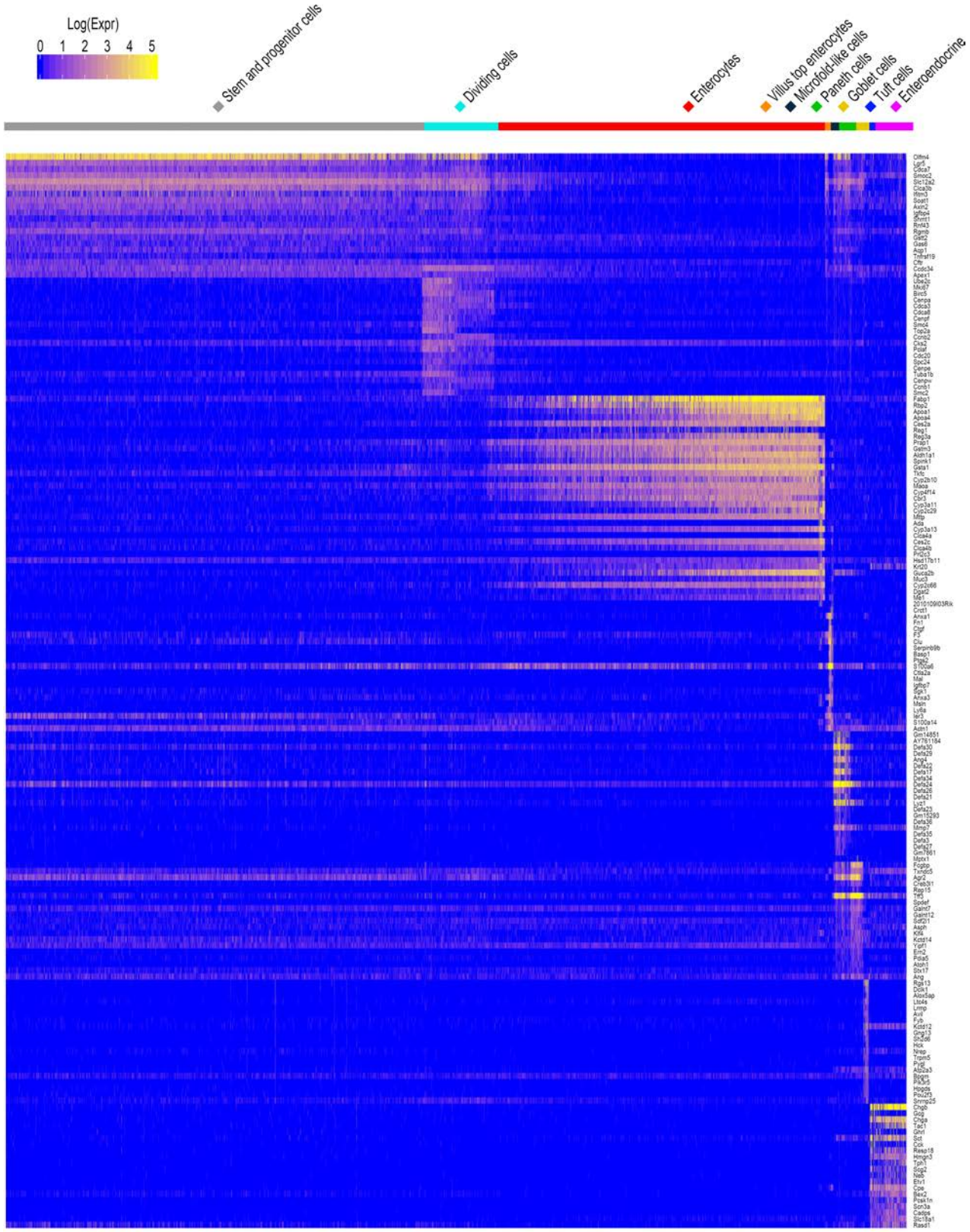

Extended Data Fig. 5 | Canonical markers from the various intestinal cell types are accurately reproduced in vitro. Heat map of unbiased top markers (Methods) associated with the various cell type clusters found in vitro. Canonical signature genes of stem cells (*Olmf4*, *Lgr5*, *Axin2*) form a continuous gradient towards enterocytes (*Fabp1*, *Apoa1*) and villus-top enterocytes (*Ada*, *Krt20*). Paneth cells express an array of antibacterial markers (defensins, lysozyme), enteroendocrine cells are marked by chromogranins (*Chga*, *Chgb*) and subpopulation-specific hormones. Tuft cells selectively express the landmark gene *Dclk1*, as well as eicosanoid biosynthesis pathway enzymes (*Alox5ap*, *Hpgds*, *Ltc4s*) and receptors implicated in taste transduction (*Trpm5*, *Gng13*).

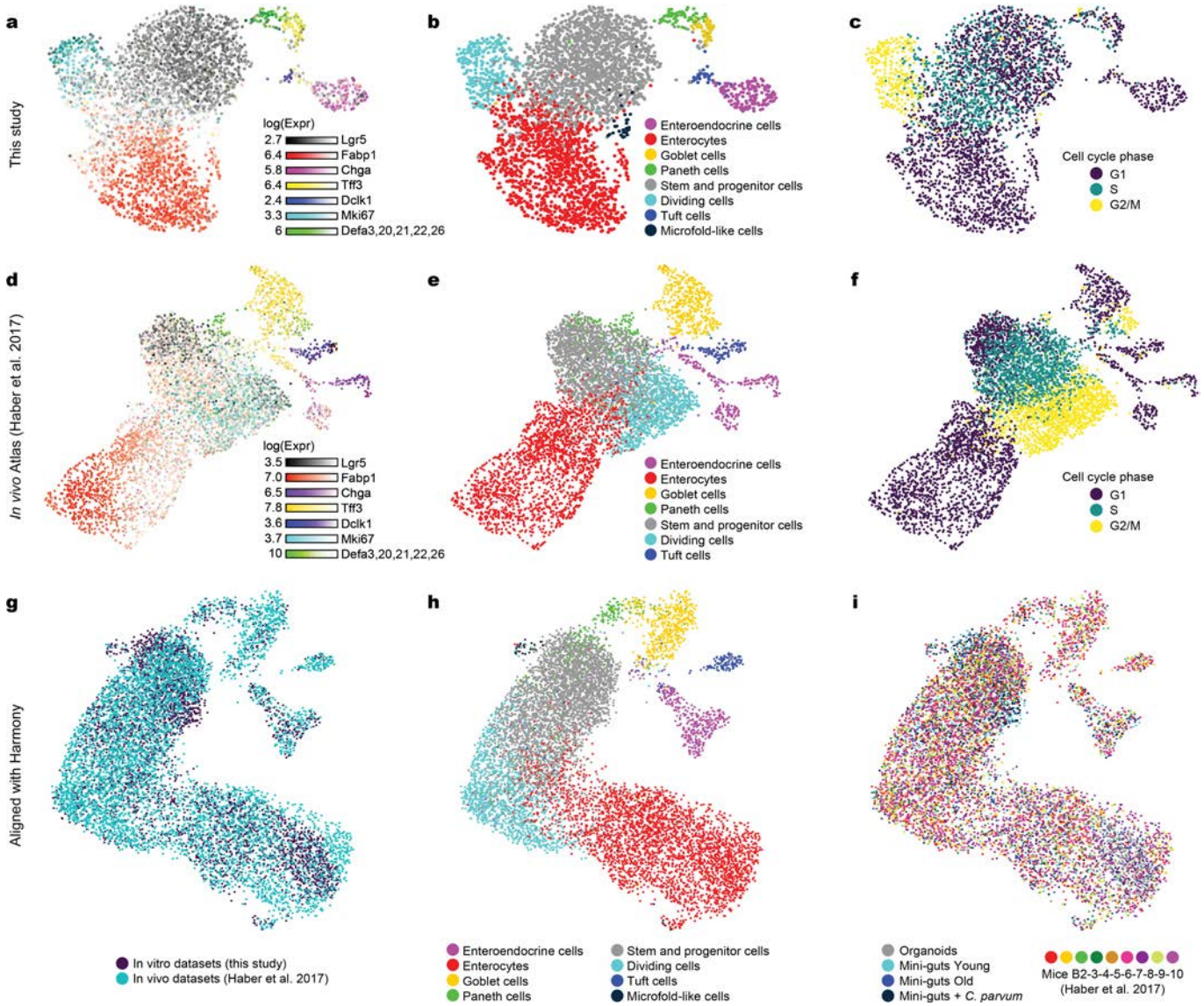

Extended Data Fig. 6 | Cell types identified in vitro closely resemble their in vivo counterparts. a–**f**, **h**, Overlay of canonical cell type markers expression (**a**, **d**), cell-cycle phase (**c**, **f**) and corresponding attributed cell types (**b**, **e**, **h**) found in vitro (**a**–**c**) and in vivo (**d**–**f**). **g**, **i**, Combined aligned in vitro and in vivo datasets showing good match between the cell types identified in the separate analyses. The in vivo versus in vitro datasets (**g**, **i**) are generated with different protocols, and gene expression values are therefore not directly comparable between the two.

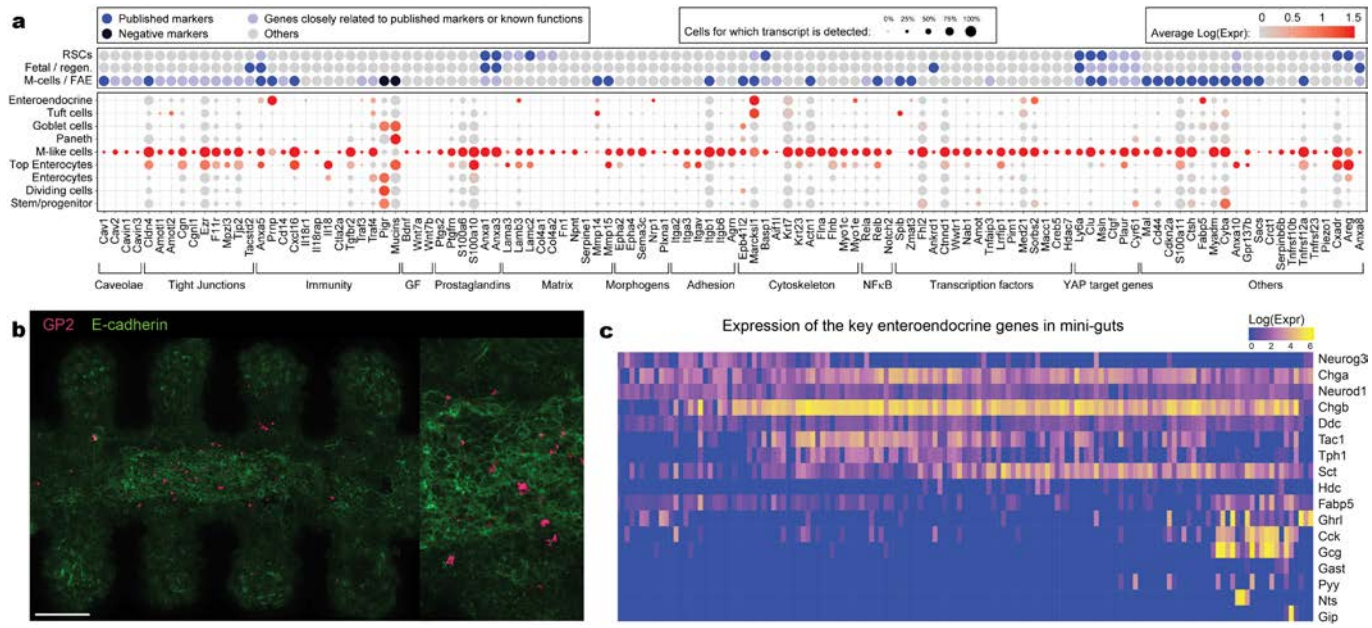

Extended Data Fig. 7 | Identification of rare cell types in the mini-guts. a, Dot plot highlighting genes relevant to the identification of the small cluster designated as microfold-like (M-like) cells that share similarities with M cells residing in follicle associated epithelia (FAE) in vivo. M-like cells express the canonical immature M-cell markers *Anxa5* and *Marcksl1*[45], involved in gram-negative bacteria binding/endocytic transport[45,46] and regulation of cytoskeleton/adhesion, respectively[47]. Other genes related to bacterial sampling are also expressed, including *Prnp*[46], *Cd14*[48] and *Aif1l*[49]. M-like cells also selectively express additional phagocytosis-related markers such as *Myadm* and *Cyba*. Notably, transcripts marking mucus secretion (sum of *Muc1*, *Muc2*, *Muc3*, *Muc3a*, *Muc4* and *Muc13*, here referred to as 'Mucins') and IgA transcytosis (*Pigr*) are missing, which is another trait of FAE[47]. Several other genes related to cytoskeleton and adhesion are also strongly upregulated in this population, including the FAE/M-cell markers *Actn1*[12,50] and *Itgb1*[49]. Additional similarities to transcripts marking M-cells include the tight junction marker *Cldn4* (Claudin 4) involved in antigen sampling/endocytosis[45,51], the caveolae marker *Cav1*[52] and the cytokine *Cxcl16*[53] that mediates lympho-epithelial interaction in gut associated lymphoid tissue[54], as well as several upregulated NFκB target genes[51]. Several other known FAE and M-cell markers are missing in these M-like cells, including *Spib*, the master controller of M-cell differentiation acting downstream of RANKL signalling[55]. This suggested that M-like cells in mini-gut tubes are only partially analogous to M-cells. We noted that our M-like cell population also shared many transcriptional similarities with two recently described, rare cell populations in the intestine, namely 'revival stem cells' (RSCs)[14,56] and regenerative fetal-like stem cell[15,56]. In particular, M-like cells in mini-guts were found to selective express the RSC markers *Clu* and *Msln*[14,56], previously reported as FAE/M-cell markers[9,46,53], and *Ly6a* (Sca1), that also defines regenerative fetal-like epithelial cells[15,56]. A characteristic feature of both RSCs and fetal-like stem cells is the activation of the YAP pathway, mediated by focal adhesions, inflammation or prostaglandin E2. Both YAP target genes and prostaglandin-related genes were found to be strongly and selectively expressed in our M-like cell population as well. **b**, Fluorescence confocal images of representative 15 days-old mini-gut tube, showing an entire tissue (left column) and a higher magnification view (right column) containing GP2$^+$ (red) M-like cells. Data are representative of two replicates. Scale bar, 100 µm. **c**, Expression of the key enteroendocrine genes in the mini-guts tubes. *Neurog3*, a marker of immature enteroendocrine cells, forms a gradient towards *Chga*, *Chgb* and *Neurod1*, marking mature enteroendocrine cells. Furthermore, a subpopulation of the enterochromaffin cells defined by hormone substance P (*Tac1*) and *Tph1*, encoding the rate-limiting enzyme in serotonin synthesis, can be detected. A subpopulation of cholecystokinin producing I-cells (*Cck*) was found, co-expressing proglucagon products (*Gcg*), and varying levels of peptide YY (*Pyy*), ghrelin (*Ghrl*) and gastrin (*Gast*). Enteroendocrine cells were also found to highly express *Wnt3*, which may partially contribute to the observed higher number of stem cells in mini-guts.

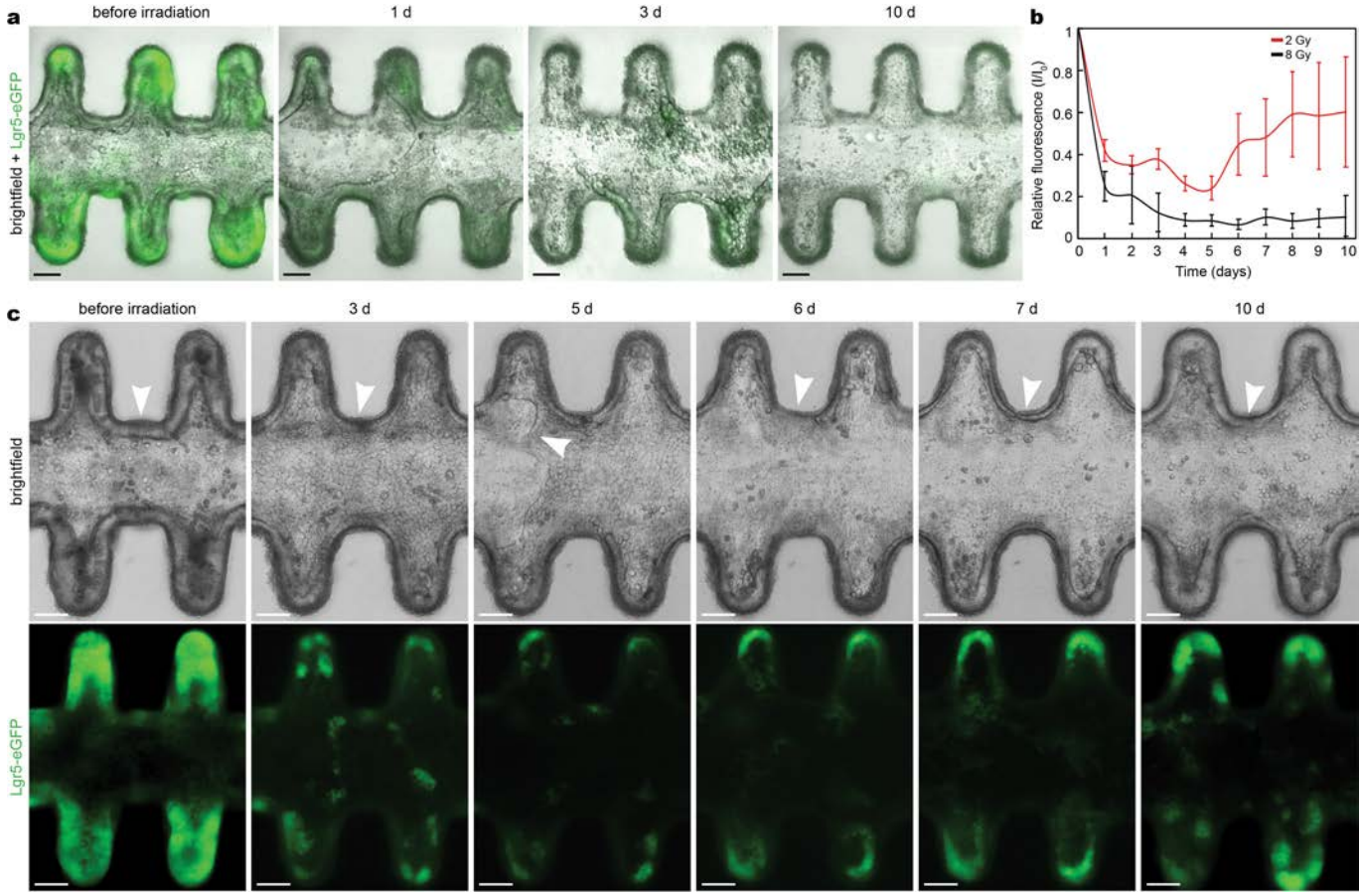

Extended Data Fig. 8 | Capacity of mini-gut tubes to regenerate after radiation-induced damage. a, Mini-gut tubes fail to regenerate and rapidly deteriorate upon exposure to 8 Gy radiation dose. Overlaid bright-field and LGR5–eGFP fluorescence time-course images of epithelial damage in mini-gut tubes induced by exposure to 8 Gy radiation dose are shown. Scale bars, 60 µm. **b**, Rapid replenishment of LGR5–eGFP^{+} stem cells initially eliminated by exposure to 2 Gy radiation dose. A graph showing normalized fluorescence intensity of eGFP measured in the crypts before and after exposure to 2 Gy and 8 Gy radiation dose. Mean ± s.d. for $n = 4$ samples. **c**, Time-course of mini-gut tubes regeneration upon 2 Gy radiation dose-induced damage shown in bright-field and LGR5–eGFP fluorescence. EDF of bright-field images, calculated for a z-stack of 80 µm; fluorescence confocal images correspond to a maximal intensity projection of a z-stack of around 60 µm. Scale bars, 60 µm. All data are representative of at least two independent experiments with $n = 3$ replicates per each condition.

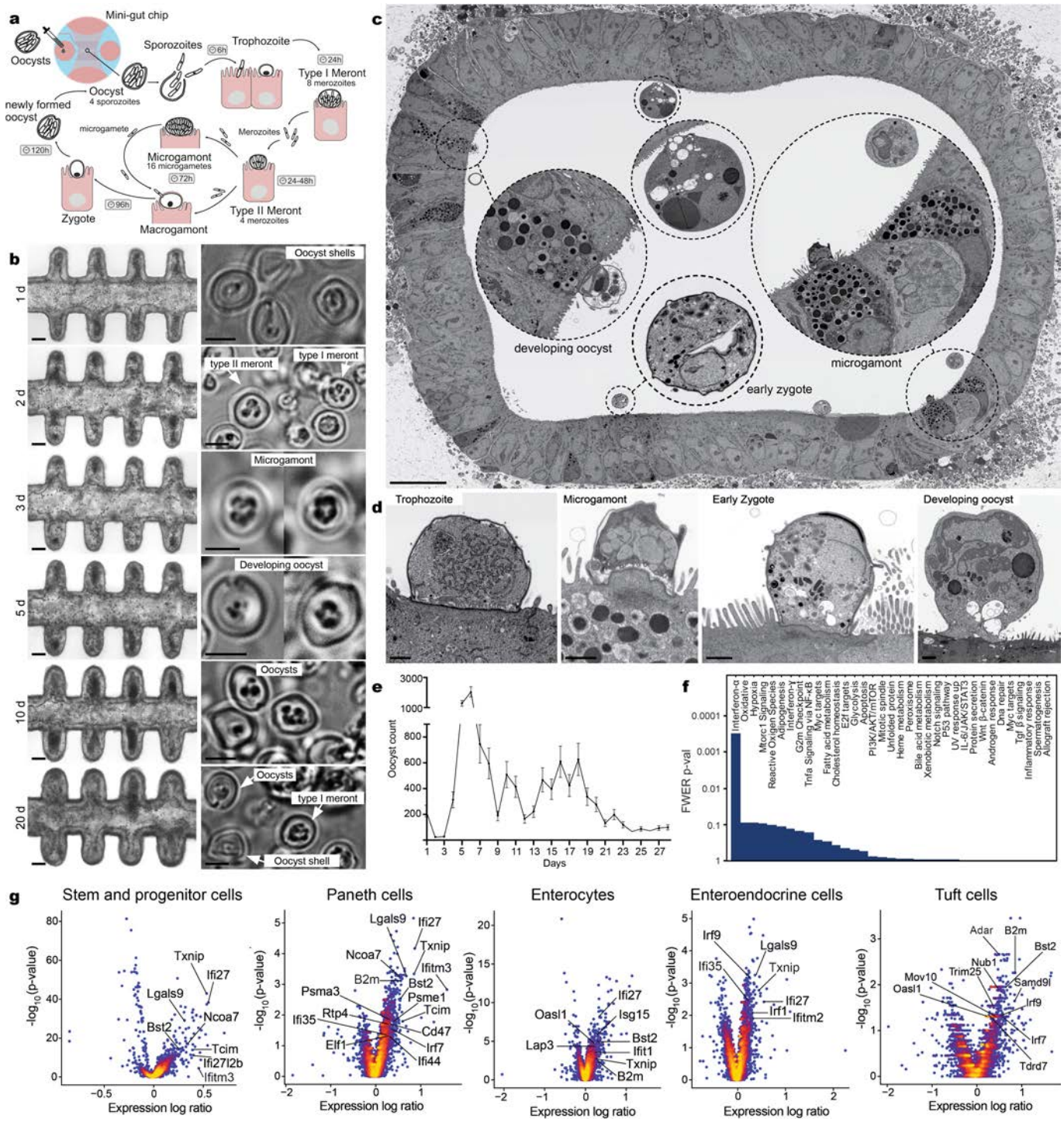

Extended Data Fig. 9 | See next page for caption.

Extended Data Fig. 9 | Modelling *C. parvum* infection in mini-gut tubes. **a**, Schematic representation of the *C. parvum* life cycle and how it can be assessed in mini-gut tube cultures. **b**, Bright-field live imaging of *C. parvum* infection in mini-guts with major epicellular stages. After about 24 h of infection, floating half-empty oocysts, broken shells and freshly excysted sporozoites were observed; on the following day, 6–8-merozoite-containing type I meronts and 4-merozoite-containing type II meronts could be detected; 3 days post infection microgamonts containing 12–16 microgametes were detected and starting from day 5 oocysts containing 1–4 sporozoites were again observed. Identity of the observed epicellular stages was confirmed by specific immunostaining (Fig. 3d). Scale bars, 3 µm. **c**, **d**, Scanning electron microscopy of distinct stages of *C. parvum* life cycle with **c**, different epicellular stages observed in a single cross-section, including microgamont, early zygote and developing oocyst in the mini-gut tubes 96 h after infection. Scale bar, 20 µm. **d**, All major epicellular stages of the *C. parvum* were observed in other samples, including trophozoite (24 h post infection), type II meront (48 h post infection) and macrogamont, early zygote and developing oocyst (72–96 h post infection). Scale bars, 1 µm. Data are representative of independent observations from one experiment. **e**, Quantification of oocysts produced in mini-gut tubes over four weeks. Mean ± s.d. for $n = 3$ replicates analysed. Data are representative of independent observations from one experiment. **f**, Hallmark pathways from the molecular signature database (MSigDB) enriched in *C.-parvum*-infected mini-guts compared to control tissues, as estimated from GSEA. The epithelium responds to the infection through interferon-α, with a family wise error rate (FWER). P value <0.001 (one-sided, empirical P value accounting for multiple testing for 50 signatures, found by integration of the tail of the null-distribution histogram generated from 10,000 phenotype permutations, $n = 961$ versus 611 cells in the comparison, from at least 3 tubes per condition, merged for RNA library construction and sequencing). **g**, Volcano plots showing differential gene expression in single cell types of infected versus control mini-guts, with interferon response genes highlighted.

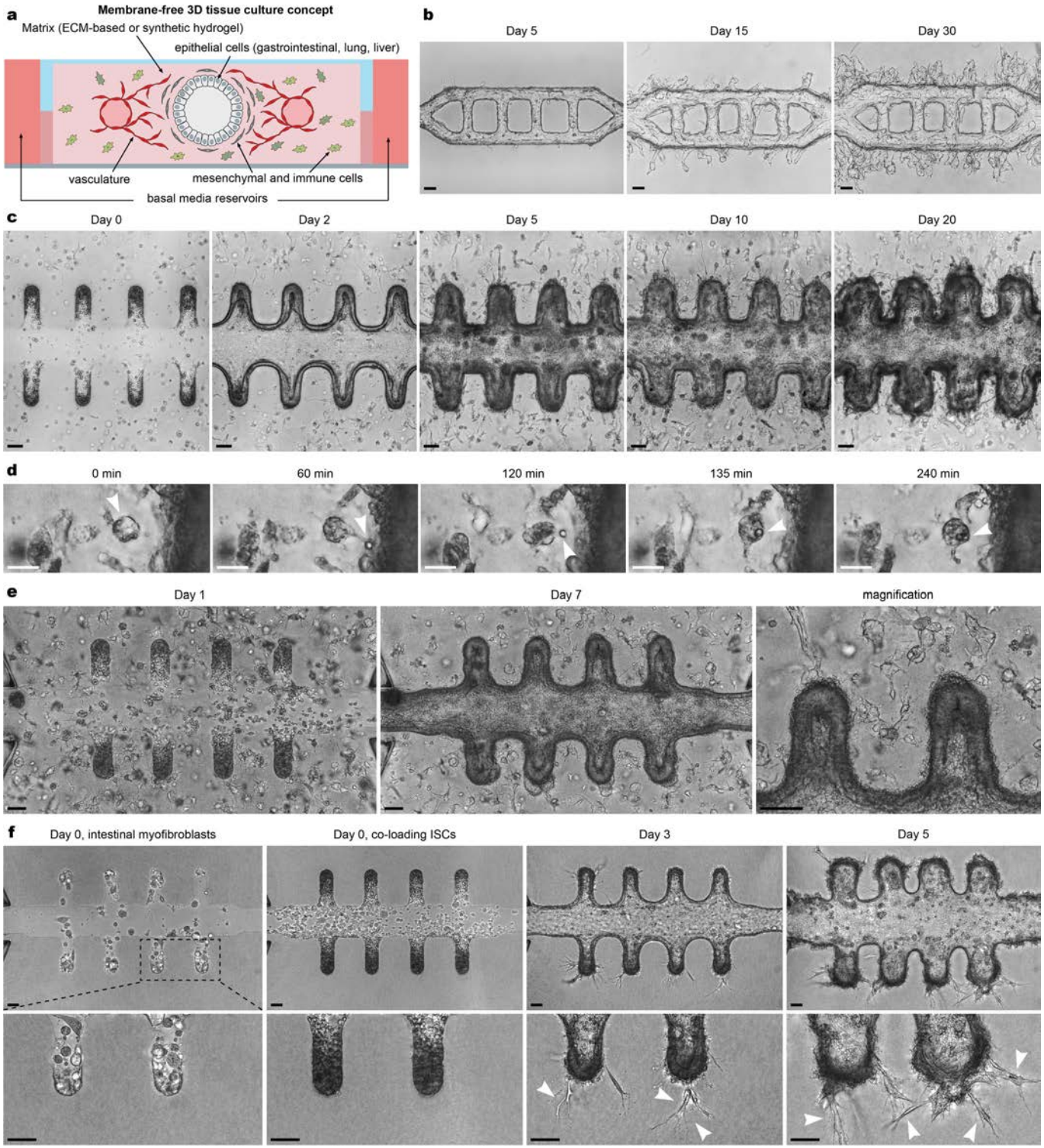

Extended Data Fig. 10 | See next page for caption.

Extended Data Fig. 10 | Perspectives for mimicking organ-level complexity in mini-gut tubes through spatially controlled co-cultures. a, A schematic representation of the 3D hydrogel-containing mini-gut chip (left). A cross-sectional view (right) highlights the solid membrane-free co-culture, in a biomimetic 3D environment, of an epithelium and various non-parenchymal cell types seeded in the matrix surrounding the epithelium. **b**, Development of engineered blood vessel-like networks composed of human endothelial cells. Scale bars, 100 µm. **c**, Co-culture experiment of mini-gut tubes with macrophages embedded into the surrounding hydrogel. Time-lapse imaging revealed a direct interaction of highly motile macrophages with intestinal epithelia in long-term co-cultures (here: 20 days). From day 2 onwards, the macrophages acquire a distinct elongated morphology and migrate towards the epithelium. Scale bars, 50 µm. **d**, Macrophages perform their phagocytic function in a co-culture with mini-guts. Higher magnification views showing a macrophage ingesting a particle from the basal side of the epithelium by phagocytosis. Scale bars, 10 µm. **e**, Mini-gut tubes co-cultured with mouse intestinal myofibroblasts incorporated in the surrounding matrix. Myofibroblasts extensively migrate through the gel, extend processes and directly interact with the epithelium. Scale bars, 50 µm. **f**, A co-culture experiment of mini-guts epithelium with myofibroblasts initially co-seeded together with ISCs directly into the lumen. Myofibroblasts rapidly attach in the microchannel and remain incorporated into the continuous monolayer generated by ISCs. From day 3 onwards, myofibroblasts, localized predominantly in crypt regions, extended pseudopodia into the surrounding matrix (arrows), recapitulating the in vivo tissue architecture. Scale bars, 50 µm. All data are representative of at least two independent experiments. EDF of bright-field images (**c**–**f**), calculated for a *z*-stack of 80 µm.